




Infrared Spectroscopy of Symbiotic Stars. XII. The Neutron Star SyXB System 4U 1700+24 = V934 Herculis

Kenneth H. Hinkle¹ , Francis C. Fekel² , Richard R. Joyce¹ , Joanna Mikołajewska³ ,
Cezary Gałań³ , and Thomas Lebzelter⁴ 

¹National Optical Astronomy Observatory, P.O. Box 26732, Tucson, AZ 85726, USA; khinkle@noao.edu, joyce@noao.edu

²Tennessee State University, Center of Excellence in Information Systems, 3500 John A. Merritt Boulevard, Box 9501, Nashville, TN 37209, USA
fekel@evans.tsuniv.edu

³Nicolaus Copernicus Astronomical Center, Polish Academy of Sciences, Bartycka 18, PL-00-716 Warsaw, Poland; mikolaj@camk.edu.pl, cgalan@camk.edu.pl

⁴University of Vienna, Department of Astrophysics, Türkenschanzstrasse 17, A-1180 Vienna, Austria; thomas.lebzelter@univie.ac.at

Received 2018 November 6; revised 2018 December 19; accepted 2018 December 20; published 2019 February 8

Abstract

The X-ray symbiotic (SyXB) V934 Her = 4U 1700+24 is an M giant–neutron star (NS) binary system. Employing optical and infrared radial velocities spanning 29 yr combined with the extensive velocities in the literature, we compute the spectroscopic orbit of the M giant in that system. We determine an orbital period of 4391 days, or 12.0 yr, the longest for any SyXB and far longer than the 404 day orbit commonly cited for this system in the literature. In addition to the 12.0 yr orbital period, we find a shorter period of 420 days, similar to the one previously found. Instead of orbital motion, we attribute this much shorter period to long secondary pulsation of the M3 III SRb variable. Our new orbit supports earlier work that concluded that the orbit is seen nearly pole-on, which is why X-ray pulsations associated with the NS have not been detected. We estimate an orbital inclination of 11.3 ± 0.4 . Arguments are made that this low inclination supports a pulsation origin for the 420 day secondary period. We also measure the CNO and Fe peak abundances of the M giant and find it to be slightly metal-poor compared to the Sun, with no trace of the NS-forming supernova event. The basic properties of the M giant and NS are derived. We discuss the possible evolutionary paths that this system has taken to get to its current state.

Key words: binaries: symbiotic – stars: abundances – stars: evolution – stars: individual (V934 Her) – stars: late-type – X-rays: binaries

Supporting material: machine-readable table

1. Introduction

Symbiotic X-ray binaries (SyXBs) are a rare class of low-mass, hard X-ray binaries consisting of a neutron star (NS) accreting mass from an M giant (Mürset et al. 1997). The much more common symbiotic systems (SySts) contain a white dwarf accreting mass from, typically, a K or M giant. The SySts are identified by emission lines in the optical that result from accretion processes. The SyXBs differ from the SySts in having nearly normal optical spectra. Unlike SySts that are found because of their optical emission lines, typical SyXBs are first identified as X-ray sources and then later associated with M-giant optical counterparts.

Since the companion to the NS is a low-mass M giant, SyXBs are also classified as low-mass X-ray binaries (LMXBs). As described by Liu et al. (2007), typical LMXBs have orbital periods of days, with the low-mass star transferring matter by Roche-lobe overflow to the NS primary. The low-mass star can be a white dwarf, a main-sequence star, or an F–G subgiant. The SyXBs differ from the larger group of LMXBs in having a giant companion to the NS, an orbital period of years, and an exceedingly slow NS spin of minutes to hours (Lü et al. 2012; Enoto et al. 2014). To date, the total number of confirmed SyXB systems is barely over a half dozen, with the Galactic population estimated to be ~ 100 –1000 (Lü et al. 2012).

While the NS must result from a supernova (SN), there are multiple possible evolutionary paths. The companion star to the NS in SyXB systems serves as a probe of the evolution of both objects. The SN event that created the NS might seem to

exclude the continued presence of a stellar companion. The zero age main sequence (ZAMS) binary progenitors of SyXBs consisted of a massive star or massive stars with a low-mass companion. The formation of the NS and the survival of the binary have been widely discussed for all types of NS binaries. For core-collapse SNe (CCSs), small asymmetries in the explosion result in large velocities for the NS remnant, and this could easily disrupt the binary (Dewey & Cordes 1987). To avoid this problem, other routes for forming the NS have been discussed, for instance, the rotationally delayed, accretion-induced collapse (AIC) of a white dwarf (Freire & Tauris 2014). Other schemes involve common-envelope phases. For a high mass–low mass system, a common-envelope stage could occur at the supergiant stage followed by the explosion of the stripped, evolved supergiant core (Taam & Sandquist 2000). Iben & Tutukov (1999) discussed an SyXB system resulting from triple system evolution. For a massive binary with a distant companion, the massive binary could undergo various merger, common-envelope, and SN events. However, population synthesis calculations favor CCSs to create the NS (Lü et al. 2012; Zhu et al. 2012).

Understanding the known systems is an obvious prerequisite to sorting out the evolutionary tracks. There is little information about either the cool star or the orbital parameters for most SyXBs. In a previous paper of this series, we undertook a detailed study of the M III in the bright X-ray SyXB, faint SySt system GX 1+4 = V2116 Oph (Hinkle et al. 2006). The GX 1+4 system has an orbital period of 3.18 yr with an NS spin period of ~ 2 minutes (González-Galán et al. 2012). Here we take a detailed look at the optical and near-IR spectra of

V934 Her = HD 154791 = 4U 1700+24. Because V934 Her is much less active than V2116 Oph, it is a more typical example of the SyXB class. Its spectrum is that of a typical early M giant with no optical emission lines (Goranskij et al. 2012). A peculiarity of this system is that no periods have been found in the X-ray data; hence, the spin period of the NS is unknown. Galloway et al. (2002) and Masetti et al. (2002) attributed this lack of an X-ray periodicity to the NS being seen close to pole-on.

We start by presenting a brief review of previous work on HD 154791. We then discuss the extensive set of velocity observations. Using these data, we determine the orbital elements of the M giant and discuss the contribution to the velocities from the stellar pulsation. This is followed by a section on stellar parameters for the M giant and an analysis of the stellar abundances. Finally, we discuss the evolution of the M giant and the binary system.

2. A Brief Review of HD 154791 = V934 Her = 4U 1700+24

The X-ray source 4U 1700+24 was discovered roughly simultaneously by Cooke et al. (1978) in Ariel V scans for high-latitude X-ray sources and Forman et al. (1978) from the Uhuru X-ray catalog. Garcia et al. (1983) found the Einstein X-ray position to be coincident with the $V = 7.6$ mag normal M giant HD 154791. Using standard models for stellar wind accretion, Garcia et al. (1983) showed that a binary model with an NS accreting mass from an M giant was a plausible explanation for the X-ray luminosity and energy distribution. Lack of velocity variations $\gtrsim 5$ km s⁻¹ over an 8 month period suggested either that the system has a very long orbital period or that it was viewed nearly face-on.

Garcia et al. (1983) found three emission lines in the *IUE* ultraviolet spectrum of HD 154791 that are not seen in normal M-giant spectra. Dal Fiume et al. (1990) found that these UV emission lines have variable strengths associated with variations in the X-ray flux, strengthening the connection with an accretion process. In addition, Brown et al. (1990) found that the He I 10830 Å line is present with strong emission and absorption. The He I 10830 Å $2^3S - 2^3P$ line has a metastable lower state 20 eV above the ground state and is diagnostic of binary star X-ray activity. However, Sokoloski et al. (2001) found no flickering in *B* with a limit of ~ 10 mmag.

Garcia et al. (1983) identified the optical spectral type of HD 154791 as M3 II. However, Masetti et al. (2002) found its spectrum to be a poor fit to standard M3 II template spectra and preferred M2 III. With standard values for the bolometric magnitude of an M2 III, a distance of 420 ± 40 pc results, in good agreement with the *Hipparcos* distance of 390 ± 130 pc. The connection of the M giant and the X-ray source was cemented by the Masetti et al. (2006) measurement of a *Chandra* position for the X-ray source with an uncertainty of $\pm 0''.6$, in excellent agreement with the optical *Hipparcos* position of the M giant. From time-series photometry provided by the *Hipparcos* team, Kazarovets et al. (1999) assigned HD 154791 the variable star name V934 Her.

Galloway et al. (2002) and Masetti et al. (2002) both noted that, assuming a typical M2 III luminosity of $550 L_{\odot}$, the M giant is about 200 times more luminous than the X-ray source. This explains the lack of rapid optical variations, since the contribution from the X-ray source is negligible compared to the M-giant optical and UV flux. This also explains why the

optical spectrum is not peculiar. In the case of the SyXB V2116 Oph/GX 1+4, an SyXB with symbiotic emission lines, the stellar luminosity is four times less than the X-ray luminosity.

The variable X-ray source component of the binary,⁵ 4U 1700+24, does not have any periods detectable in the 2–2700 s range (Garcia et al. 1983). Galloway et al. (2002) similarly concluded that 4U 1700+24 is different from other NSs detected in the X-ray region, since no coherent or quasi-periodic oscillations could be seen in the X-ray data. Masetti et al. (2002) confirmed that 4U 1700+24 has substantial X-ray variability, but this lacks periodicity. This paper and Galloway et al. (2002) both concluded that the lack of periodicity results from viewing the NS nearly pole-on with the magnetic axis aligned to the NS spin axis. In this geometry, hot spots on the NS will be continuously in view.

Masetti et al. (2002) found the size of the X-ray-emitting area to be on the order of tens of m. This suggests that the accretion is funneled by the magnetic field onto the magnetic polar cap. Masetti et al. (2002) noted that the presence of an M-giant wind was inferred from both the UV variability and the IRAS 12 and 25 μ m measurements of a mid-IR excess. An accretion rate of $\sim 10^{-14} M_{\odot} \text{ yr}^{-1}$ was shown to be consistent with normal values for both a red giant mass-loss rate, $\sim 10^{-9} M_{\odot} \text{ yr}^{-1}$, and an accretion efficiency onto an NS of $\sim 10^{-4}$.

Galloway et al. (2002) acquired high-resolution spectra of V934 Her in a 44 Å region around 5200 Å on 83 occasions. Their observations span nearly 15 yr starting in 1982. A search for periods in the 50–1000 day range found a 3.3σ period at about 410 days. An elliptical orbit was then fit to the data, resulting in a 404 ± 3 day period. That orbit had a semi-amplitude of 0.75 ± 0.12 km s⁻¹ and an eccentricity of 0.26. Given an orbital period of ~ 400 days and typical masses of $1.4 M_{\odot}$ for the NS and $1.3 M_{\odot}$ for the M giant, Masetti et al. (2002) found from Kepler's third law a semimajor axis of $\sim 300 R_{\odot}$ and an orbital velocity of ~ 30 km s⁻¹. An inclination of $\lesssim 5^{\circ}$ is required to match the observed velocity amplitude. The probability that a binary inclination will be less than or equal to an inclination i is $1 - \cos(i)$. An inclination of 5° or less has a probability of less than 0.5%.

Tiengo et al. (2005) identified the O VIII Ly α line redshifted by ~ 3500 km s⁻¹ at 19.19 Å in the X-ray spectrum of 4U 1700+24. They found that this is in agreement with the emitting gas being accreted by the NS at the magnetospheric radius. Nucita et al. (2014) found that this is ~ 1000 km above the NS. Again, the requirement is that the system is observed nearly pole-on, with the magnetic and rotation poles aligned. The O VIII line observation was confirmed by Nucita et al. (2014). They endorsed both the small size of the X-ray-emitting area and the nearly pole-on aspect of the NS. Both González-Galán et al. (2012) and Lü et al. (2012) argued that mass transfer in SyXBs occurs through quasi-spherical wind accretion flowing along NS magnetic field lines. Thus, the SyXBs differ from symbiotic binaries in not having accretion disks. In the case of quasi-spherical accretion, rather than disk accretion, the prominent optical emission features associated with disk accretion are not present. Krimm et al. (2014) and Burrows et al. (2015) reported on a series of X-ray flares observed by *Swift* where the

⁵ In this paper, we refer to the SyXB system observed in the optical and infrared as V934 Her and reserve the name 4U 1700+24 for the X-ray source. However, as reflected in the title of this paper, the optical and X-ray names are fully synonymous throughout most of the literature.

Table 1
Radial Velocities of V934 Her

Helio. JD – 2,400,000	RV (km s ^{–1})	$O - C$ (km s ^{–1})	ϕ_L	RV _L (km s ^{–1})	ϕ_S	RV _S (km s ^{–1})	Source ^a
45,072.3976	–47.37	1.22	0.256	–47.63	0.483	1.48	CfA
45,153.2525	–47.11	1.88	0.275	–46.96	0.676	1.73	CfA
45,153.2592	–47.22	1.77	0.275	–47.07	0.676	1.62	CfA
45,242.1427	–49.52	0.02	0.295	–48.80	0.887	–0.70	CfA
45,427.4203	–51.30	–3.03	0.337	–51.77	0.328	–2.56	CfA
45,427.4545	–49.01	–0.74	0.337	–49.48	0.328	–0.27	CfA
45,450.3925	–47.91	0.41	0.343	–48.32	0.383	0.82	CfA
45,754.5360	–48.79	–0.56	0.412	–49.07	0.107	–0.28	CfA
47,345.6300	–46.65	0.36	0.774	–45.92	0.894	–0.37	KPNO1 ^b
48,408.3953	–45.95	–0.22	0.016	–46.30	0.423	0.13	CfA
48,431.2564	–46.73	–0.79	0.021	–47.00	0.477	–0.52	CfA
48,672.5247	–47.69	–0.14	0.076	–47.64	0.052	–0.19	CfA
48,695.5450	–46.72	0.60	0.082	–47.00	0.106	0.88	CfA
48,723.4965	–46.37	0.87	0.088	–46.85	0.173	1.35	CfA
48,752.4824	–47.13	0.18	0.095	–47.65	0.242	0.70	CfA
48,783.3251	–46.55	0.91	0.102	–47.03	0.315	1.39	CfA
48,818.2600	–47.37	0.30	0.110	–47.76	0.398	0.69	CfA
48,839.1402	–48.24	–0.43	0.114	–48.55	0.448	–0.11	CfA
48,874.1625	–49.62	–1.56	0.122	–49.79	0.532	–1.39	CfA
48,903.0909	–48.92	–0.65	0.129	–48.95	0.600	–0.62	CfA
49,048.4257	–49.83	–0.52	0.162	–49.11	0.946	–1.24	CfA
49,086.3421	–49.36	–0.55	0.171	–49.19	0.037	–0.72	CfA
49,107.3136	–48.70	–0.21	0.175	–48.88	0.086	–0.03	CfA
49,137.2635	–47.83	0.42	0.182	–48.28	0.158	0.87	CfA
49,167.1858	–48.33	–0.12	0.189	–48.85	0.229	0.40	CfA
49,196.1055	–47.94	0.32	0.196	–48.44	0.298	0.81	CfA
49,230.1082	–48.62	–0.26	0.203	–49.03	0.379	0.16	CfA
49,256.0466	–48.27	0.20	0.209	–48.60	0.440	0.52	CfA
49,263.9965	–49.03	–0.53	0.211	–49.33	0.459	–0.23	CfA
49,271.9952	–49.65	–1.11	0.213	–49.91	0.478	–0.85	CfA
49,284.9803	–48.76	–0.16	0.216	–48.97	0.509	0.05	CfA
49,317.9145	–48.95	–0.19	0.223	–49.01	0.588	–0.13	CfA
49,374.4494	–50.34	–1.23	0.236	–50.07	0.722	–1.50	CfA
49,388.4426	–49.80	–0.60	0.239	–49.44	0.756	–0.96	CfA
49,401.4404	–51.15	–1.85	0.242	–50.70	0.786	–2.31	CfA
49,418.4181	–50.62	–1.20	0.246	–50.05	0.827	–1.78	CfA
49,430.4187	–50.15	–0.65	0.249	–49.50	0.855	–1.31	CfA
49,448.3694	–49.55	0.03	0.253	–48.81	0.898	–0.70	CfA
49,459.3857	–49.71	–0.12	0.256	–48.96	0.924	–0.86	CfA
49,473.3215	–48.72	0.81	0.259	–48.03	0.958	0.13	CfA
49,494.2598	–50.13	–0.88	0.264	–49.73	0.007	–1.29	CfA
49,495.2301	–49.61	–0.38	0.264	–49.23	0.010	–0.77	CfA
49,504.3172	–48.91	0.15	0.266	–48.70	0.031	–0.07	CfA
49,519.2388	–49.14	–0.35	0.269	–49.20	0.067	–0.30	CfA
49,536.2015	–48.86	–0.31	0.273	–49.15	0.107	–0.02	CfA
49,548.1608	–49.61	–1.16	0.276	–50.00	0.136	–0.77	CfA
49,565.1973	–48.69	–0.34	0.280	–49.17	0.176	0.14	CfA
49,590.0435	–49.25	–0.94	0.285	–49.77	0.235	–0.42	CfA
49,596.0637	–48.36	–0.05	0.287	–48.88	0.250	0.47	CfA
49,607.0952	–48.67	–0.36	0.289	–49.18	0.276	0.15	CfA
49,617.0588	–48.58	–0.25	0.292	–49.08	0.300	0.24	CfA
49,638.9850	–49.46	–1.09	0.297	–49.91	0.352	–0.64	CfA
49,756.4591	–48.92	–0.11	0.323	–48.88	0.631	–0.15	CfA
49,766.3693	–48.46	0.40	0.326	–48.36	0.655	0.30	CfA
49,796.4229	–49.60	–0.57	0.332	–49.32	0.727	–0.85	CfA
49,815.3620	–48.51	0.64	0.337	–48.10	0.772	0.23	CfA
49,845.3133	–49.59	–0.25	0.344	–48.97	0.843	–0.87	CfA
49,852.2900	–48.55	0.83	0.345	–47.89	0.859	0.17	CfA
49,874.1502	–47.44	2.01	0.350	–46.69	0.911	1.27	CfA
49,888.2834	–48.52	0.90	0.353	–47.80	0.945	0.18	CfA
49,902.1412	–48.96	0.32	0.356	–48.37	0.978	–0.27	CfA
49,909.1852	–49.16	0.02	0.358	–48.67	0.995	–0.48	CfA
49,918.2127	–48.12	0.89	0.360	–47.79	0.016	0.56	CfA

Table 1
(Continued)

Helio. JD – 2,400,000	RV (km s ⁻¹)	$O - C$ (km s ⁻¹)	ϕ_L	RV _L (km s ⁻¹)	ϕ_S	RV _S (km s ⁻¹)	Source ^a
49,939.1151	-48.36	0.25	0.365	-48.41	0.066	0.31	CfA
49,949.1086	-48.31	0.15	0.367	-48.51	0.090	0.35	CfA
49,965.1146	-47.87	0.41	0.371	-48.24	0.128	0.78	CfA
49,973.0348	-47.69	0.53	0.373	-48.11	0.147	0.95	CfA
49,992.0428	-48.07	0.06	0.377	-48.57	0.192	0.56	CfA
50,007.9674	-49.55	-1.45	0.381	-50.07	0.230	-0.93	CfA
50,027.9450	-48.42	-0.33	0.385	-48.93	0.278	0.18	CfA
50,112.4585	-47.80	0.47	0.404	-48.06	0.479	0.74	CfA
50,141.4002	-49.08	-0.70	0.411	-49.22	0.548	-0.56	CfA
50,157.4025	-48.05	0.39	0.415	-48.11	0.586	0.45	CfA
50,183.3229	-47.91	0.65	0.421	-47.83	0.647	0.57	CfA
50,203.2546	-49.02	-0.36	0.425	-48.82	0.695	-0.56	CfA
50,211.3116	-48.90	-0.20	0.427	-48.65	0.714	-0.44	CfA
50,236.2234	-49.50	-0.65	0.433	-49.09	0.773	-1.07	CfA
50,262.2075	-49.60	-0.59	0.438	-49.00	0.835	-1.19	CfA
50,276.1672	-48.76	0.32	0.442	-48.08	0.868	-0.36	CfA
50,288.1864	-48.85	0.27	0.444	-48.12	0.897	-0.46	CfA
50,319.1151	-48.56	0.43	0.451	-47.93	0.971	-0.20	CfA
50,348.0109	-47.59	0.89	0.458	-47.44	0.039	0.74	CfA
50,362.9830	-47.57	0.64	0.461	-47.68	0.075	0.75	CfA
50,382.9624	-47.45	0.50	0.466	-47.80	0.122	0.85	CfA
51,738.776	-45.90	-0.08	0.775	-46.35	0.349	0.37	KPNO2 ^c
51,831.576	-45.20	0.78	0.796	-45.29	0.570	0.87	KPNO3
52,049.157	-45.20	0.20	0.845	-45.39	0.088	0.39	MSO
52,098.992	-45.80	-0.83	0.857	-46.31	0.207	-0.32	MSO
52,134.992	-45.00	-0.10	0.865	-45.50	0.292	0.40	MSO
52,357.318	-45.40	0.20	0.916	-44.84	0.821	-0.35	MSO
52,402.223	-45.20	0.56	0.926	-44.46	0.928	-0.18	MSO
52,447.045	-45.70	-0.50	0.936	-45.52	0.035	-0.68	MSO
52,749.825	-47.80	-1.61	0.005	-47.44	0.756	-1.97	GemS ^d
53,129.782	-46.40	1.49	0.092	-46.29	0.660	1.38	KPNO4
53,130.774	-47.10	0.80	0.092	-46.99	0.662	0.68	KPNO4
53,131.799	-47.30	0.61	0.092	-47.18	0.665	0.49	KPNO4
53,178.755	-47.10	1.29	0.103	-46.68	0.776	0.86	KPNO4
53,493.802	-47.90	0.58	0.175	-48.08	0.526	0.76	KPNO4
53,537.877	-48.00	0.75	0.185	-47.96	0.631	0.71	KPNO4
53,859.860	-48.20	0.26	0.258	-48.59	0.397	0.65	KPNO4
53,899.790	-47.40	1.20	0.267	-47.64	0.493	1.44	KPNO4
54,230.902	-48.40	-0.18	0.342	-48.91	0.281	0.33	KPNO4
54,270.753	-48.30	-0.02	0.351	-48.72	0.375	0.40	KPNO4
54,592.774	-48.00	0.05	0.425	-48.41	0.142	0.46	KPNO4
54,634.732	-46.50	1.41	0.434	-47.02	0.242	1.93	KPNO4
54,636.814	-47.10	0.81	0.435	-47.62	0.247	1.33	KPNO4
54,956.864	-49.10	-0.60	0.508	-48.71	0.008	-1.00	KPNO4
54,998.716	-48.30	-0.53	0.517	-48.59	0.108	-0.24	KPNO4
55,320.783	-48.00	0.35	0.591	-47.30	0.874	-0.34	KPNO4
55,321.715	-48.50	-0.14	0.591	-47.80	0.877	-0.84	KPNO4
55,362.751	-48.70	-0.49	0.600	-48.09	0.974	-1.10	KPNO4
55,363.758	-48.60	-0.40	0.600	-48.00	0.977	-1.00	KPNO4
55,693.744	-47.70	-0.22	0.676	-47.32	0.762	-0.60	KPNO4
55,694.722	-47.10	0.38	0.676	-46.71	0.764	-0.01	KPNO4
55,727.665	-48.00	-0.34	0.683	-47.38	0.843	-0.96	KPNO4
55,728.678	-47.40	0.26	0.684	-46.78	0.845	-0.36	KPNO4
56,055.748	-46.80	-0.35	0.758	-46.78	0.624	-0.38	KPNO4
56,058.771	-46.90	-0.44	0.759	-46.86	0.631	-0.48	KPNO4
56,086.865	-47.70	-1.14	0.765	-47.50	0.698	-1.34	KPNO2 ^c
56,087.748	-46.70	-0.13	0.765	-46.49	0.700	-0.34	KPNO2 ^f
56,099.697	-46.50	0.12	0.768	-46.21	0.728	-0.17	KPNO4
56,419.693	-44.50	0.89	0.841	-44.75	0.490	1.13	KPNO4
56,419.766	-45.50	-0.11	0.841	-45.74	0.490	0.13	KPNO4
56,420.750	-45.30	0.09	0.841	-45.54	0.492	0.33	KPNO4
56,783.698	-44.20	0.38	0.924	-44.64	0.356	0.82	KPNO4
56,785.764	-44.00	0.59	0.924	-44.44	0.361	1.02	KPNO4

Table 1
(Continued)

Helio. JD – 2,400,000	RV (km s ⁻¹)	$O - C$ (km s ⁻¹)	ϕ_L	RV _L (km s ⁻¹)	ϕ_S	RV _S (km s ⁻¹)	Source ^a
56,825.669	-44.90	-0.19	0.933	-45.20	0.456	0.11	KPNO4
56,906.677	-46.00	-0.85	0.952	-45.92	0.649	-0.93	KPNO5 ^g
57,059.966	-45.00	0.82	0.987	-44.65	0.014	0.46	Fair
57,083.951	-45.30	0.18	0.992	-45.38	0.071	0.26	Fair
57,106.882	-45.10	0.21	0.997	-45.46	0.125	0.56	Fair
57,174.700	-44.80	0.70	0.013	-45.30	0.287	1.20	Fair
57,416.020	-47.40	0.58	0.068	-46.73	0.861	-0.08	Fair
57,432.955	-48.30	-0.16	0.072	-47.56	0.901	-0.90	Fair
57,442.031	-48.70	-0.51	0.074	-47.95	0.923	-1.26	Fair
57,451.878	-48.30	-0.09	0.076	-47.58	0.947	-0.81	Fair
57,462.001	-48.60	-0.43	0.078	-47.97	0.971	-1.07	Fair
57,470.990	-48.60	-0.51	0.080	-48.09	0.992	-1.03	Fair
57,481.825	-48.30	-0.36	0.083	-47.98	0.018	-0.68	Fair
57,491.778	-48.40	-0.60	0.085	-48.27	0.041	-0.74	Fair
57,501.968	-47.40	0.26	0.087	-47.45	0.066	0.31	Fair
57,505.970	-47.40	0.21	0.088	-47.51	0.075	0.32	Fair
57,508.976	-47.90	-0.32	0.089	-48.06	0.082	-0.16	Fair
57,509.786	-47.60	-0.03	0.089	-47.77	0.084	0.14	Fair
57,514.707	-48.00	-0.47	0.090	-48.23	0.096	-0.24	Fair
57,515.845	-47.20	0.32	0.091	-47.45	0.099	0.56	Fair
57,517.789	-47.30	0.20	0.091	-47.57	0.103	0.47	Fair
57,524.813	-47.40	0.06	0.093	-47.74	0.120	0.40	Fair
57,527.783	-47.50	-0.06	0.093	-47.87	0.127	0.31	Fair
57,528.942	-48.00	-0.56	0.094	-48.37	0.130	-0.19	Fair
57,530.737	-48.10	-0.67	0.094	-48.49	0.134	-0.28	Fair
57,532.678	-48.20	-0.77	0.094	-48.60	0.139	-0.37	Fair
57,535.865	-48.00	-0.58	0.095	-48.42	0.146	-0.16	Fair
57,537.670	-47.60	-0.19	0.096	-48.03	0.151	0.25	Fair
57,538.693	-47.40	0.01	0.096	-47.84	0.153	0.45	Fair
57,539.670	-47.40	0.01	0.096	-47.84	0.155	0.46	Fair
57,542.671	-47.00	0.41	0.097	-47.46	0.163	0.87	Fair
57,544.808	-46.80	0.61	0.097	-47.27	0.168	1.07	Fair
57,545.764	-46.90	0.51	0.097	-47.37	0.170	0.98	Fair
57,546.725	-46.80	0.61	0.098	-47.27	0.172	1.08	Fair
57,547.672	-47.30	0.11	0.098	-47.78	0.174	0.58	Fair
57,554.783	-47.10	0.31	0.099	-47.60	0.191	0.81	Fair
57,577.688	-47.90	-0.43	0.105	-48.42	0.246	0.09	Fair
57,617.823	-48.10	-0.44	0.114	-48.56	0.341	0.02	Fair
57,761.018	-48.90	-0.27	0.146	-48.74	0.682	-0.43	Fair
57,781.997	-49.60	-0.79	0.151	-49.30	0.732	-1.09	Fair
57,860.987	-49.70	-0.32	0.169	-48.95	0.920	-1.07	Fair
57,878.716	-49.60	-0.28	0.173	-48.93	0.962	-0.95	Fair
57,895.906	-48.50	0.61	0.177	-48.07	0.003	0.17	Fair
57,916.838	-47.90	0.84	0.182	-47.86	0.053	0.80	Fair
57,935.891	-47.80	0.67	0.186	-48.04	0.098	0.92	Fair
58,028.686	-48.80	-0.49	0.207	-49.28	0.319	-0.01	Fair

Notes.

^a CfA = Center for Astrophysics, KPNO1 = KPNO 4 m + FTS, KPNO2 = KPNO 2.1 m + Phoenix, KPNO3 = KPNO coude feed + NICMASS, MSO = Mount Stromlo Observatory 1.88 m + NICMASS, GemS = Gemini South 8 m + Phoenix, KPNO4 = KPNO coude feed + LB1A, KPNO5 = KPNO 4 m + Phoenix, Fair = Fairborn Observatory.

^b 2.335 μm .

^c 1.557 μm .

^d 2.226 μm , $R = 70,000$.

^e 2.311 μm .

^f 1.562 μm .

^g 1.563 μm .

(This table is available in machine-readable form.)

radiation became harder as the luminosity increased. In agreement with the other models for 4U 1700+24, the analysis requires an extremely compact accretor.

3. New Observations and Reductions

We observed the spectrum of V934 Her at high resolution in the optical and near-infrared on 90 occasions using five

telescopes at four different observatories with six different instruments (Table 1). The extensive set of observations was made possible because V934 Her is bright, $K \sim 3$ mag, in the near-infrared but not so bright as to be unobservable with large telescopes. The initial observation in our data set was obtained in 1988 July. However, our monitoring of V934 Her started more than a decade later on 2000 July 13, when we observed a section of its H -band spectrum with the Phoenix cryogenic echelle spectrograph at the $f/15$ focus of the Kitt Peak National Observatory (KPNO) 2.1 m telescope. The most recent set of velocity observations, which continued into 2017, were acquired with the Fairborn 2 m telescope and fiber-fed echelle spectrograph. Thus, our velocity data set spans 29 yr.

The first observation reported here was obtained with the KPNO 4 m telescope and Fourier transform spectrometer (FTS) on 1988 July 3 as part of a program to study abundances. While FTS observations are a gold standard free from systematics in both frequencies and intensities, the technique suffers from multiplex disadvantage and is best applied to bright stars (Ridgway & Hinkle 1987). The spectrum covers the K band at an apodized resolution, $R = \lambda/\Delta\lambda$, of $\sim 32,000$. The peak signal-to-noise ratio (S/N) is 63 and required a 70 minute exposure. The 4 m FTS is discussed by Hall et al. (1978), and the reduction techniques are discussed by Hinkle et al. (1982). In addition to using the FTS observation to determine a radial velocity, the spectrum was ratioed to a spectrum of α Lyr that was observed on the same night. We analyzed this ratioed spectrum as part of our abundance analysis. The FTS spectrum was also convolved to a resolution of 1.4 cm^{-1} ($R \sim 3000$) to compare it with Wallace & Hinkle (1997) spectra of normal field stars.

The Phoenix data were acquired with either the KPNO 2.1 or 4 m telescopes or the Gemini South 8 m telescope. A complete description of the spectrograph can be found in Hinkle et al. (1998). The Gemini South observation has the highest resolving power, $R = 70,000$. The other four Phoenix observations were taken with the widest slit, resulting in $R = 50,000$. Phoenix spectra cover a small, 0.5%, wavelength interval in several regions of the H and K bands.

In 2000 October, we observed a section of the H -band spectrum using the KPNO 0.9 m coudé-feed telescope and coudé spectrograph. The detector was an infrared camera, NICMASS, developed at the University of Massachusetts. The 2 pixel resolving power was 44,000 with the observation centered at $1.623 \mu\text{m}$. Observations of V934 Her were also made with the same detector, order-sorting filter, and support electronics at the Mount Stromlo Observatory (MSO) 1.88 m telescope and coudé spectrograph in 2001 and 2002. In the MSO data, the 2 pixel resolving power is 24,000. The experimental setup that used the NICMASS camera is described in Joyce et al. (1998) and Fekel et al. (2000). The Canberra-area bush fires of 2003 January destroyed the MSO 1.88 m telescope, spectrograph, and NICMASS camera.

Following the loss of our equipment in Australia, we continued observations at KPNO using the 0.9 m coudé-feed telescope, coudé spectrograph, and a CCD designated LB1A. The 1980×800 pixel CCD was manufactured by Lawrence Berkeley National Laboratory and is $300 \mu\text{m}$ thick. Our spectrograms, centered near $1.005 \mu\text{m}$, have a wavelength range of 420 \AA and a resolving power of $\sim 21,500$. The coudé feed was closed as a result of NSF budget cuts in 2014.

As noted above, unlike typical SySts, the optical spectrum of V934 Her does not contain conspicuous emission lines or extensive veiling caused by continuum emission. As a result, for V934 Her, it is possible to acquire useful optical spectra and measure the radial velocities of the M giant without complications. Thus, in 2015 February, observations were commenced with the Tennessee State University 2 m Automatic Spectroscopic Telescope (AST) and fiber-fed echelle spectrograph (Eaton & Williamson 2007). The detector is a Fairchild 486 CCD that has a 4096×4096 array of $15 \mu\text{m}$ pixels (Fekel et al. 2013). Forty-eight echelle orders are covered, ranging in wavelength from 3800 to 8260 \AA . The observations were made with a fiber that produces a resolving power of $\sim 25,000$ at 6000 \AA .

For the near-IR spectra, standard observing and reduction techniques were used (Joyce 1992). Wavelength calibration of Phoenix, KPNO coudé, and MSO coudé data posed a challenge because the spectral coverage is too small to include a sufficient number of ThAr emission lines for a dispersion solution. Our approach was to utilize absorption lines in a K giant to obtain a dispersion solution. Several sets of lines were tried, including CO, Fe I, and Ti I. These groups all gave consistent results.

The radial velocities of the program stars for the KPNO, MSO, and Gemini South spectra were determined with the IRAF cross-correlation program FXCOR (Fitzpatrick 1993). The reference star was δ Oph, an M-giant IAU velocity standard, for which we adopted a radial velocity of -19.1 km s^{-1} from the work of Scarfe et al. (1990).

Fekel et al. (2009) provided a general explanation of the velocity measurement of AST spectra. In the particular case of V934 Her, we selected a subset of 40 lines from our solar-type star line list that are relatively unblended in M-giant spectra and range in wavelength from 5000 to 6800 \AA . Our unpublished velocities of several IAU radial velocity standards from spectra obtained with the 2 m AST have an average velocity difference of -0.6 km s^{-1} when compared to the results of Scarfe et al. (1990). Thus, we have added 0.6 km s^{-1} to each of our AST velocities.

Figure 1 plots all of our velocities, as well as those from the Center for Astrophysics (CfA) that were provided by D. Galloway (2017, private communication) and are discussed in Section 4.

On 2018 April 22, we obtained a spectrum of the H and K region of V934 Her at $R = 45,000$ using IGRINS (Park et al. 2014) on Gemini South. The integration time was a few s, so the spectrum does not contain OH night-sky lines for velocity calibration. While the wavelength/velocity calibration could be done using telluric absorption lines, for the current paper, we opted to use this spectrum only for abundance analysis. Since the spectrum has larger wavelength coverage than even the archival FTS spectrum, it became a key element in the abundance analysis. We used the pipeline-reduced IGRINS spectrum, and to fit the continuum, we used the IRAF continuum routine *splot 't'* at low order. For our analysis, it was necessary to join the echelle orders to produce K - and H -band spectra. We did this by comparing the overlap regions between the orders. Our H -band analysis of this spectrum is based on the $1.5\text{--}1.7 \mu\text{m}$ region that is utilized by the APOGEE project (Majewski et al. 2016). Use of this region was facilitated by the comprehensive line list developed by APOGEE (Shetrone et al. 2015).

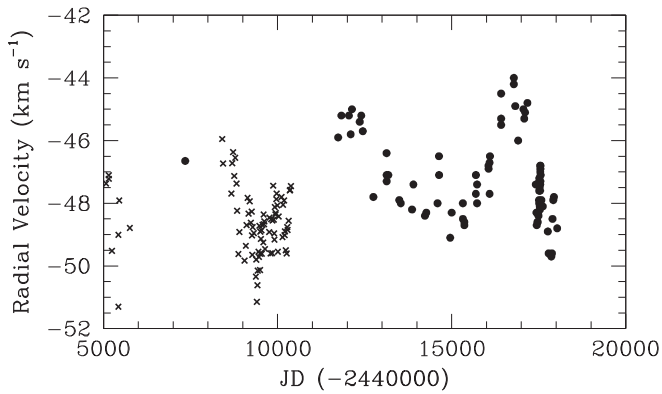


Figure 1. Radial velocity data (Table 1) for V934 Her as a function of time. Circles: our velocities; crosses: CfA.

In addition to the IGRINS spectrum, we selected seven other spectra for use in our chemical abundance analysis of V934 Her. In Table 2, the observational details of the abundance analysis spectra are provided. An identifier (first column) is given, which will be used later when it is necessary to specify individual spectra. We analyzed the FTS spectrum, since it covers the entire K band roughly 20 yr prior to the IGRINS observation. However, both the S/N and resolution are inferior to the IGRINS spectrum. To supplement these data, we also included two K -band Phoenix spectra that cover narrower (~ 100 Å) regions, one at $2.31 \mu\text{m}$ and a second at $2.22 \mu\text{m}$, and three H -band Phoenix spectra that cover a narrow region (~ 65 Å) at $\sim 1.56 \mu\text{m}$. For all of the abundance data, a telluric reference spectrum of a hot star was observed at approximately the same time. With this reference spectrum, the telluric lines have been ratioed from the V934 Her spectra.

4. Orbital Elements

The observed velocities (Figure 1) suggest a long-period orbit. We searched for an orbital period in our radial velocity data using the least-string method as implemented by T. Deeming (PDFND; Bopp et al. 1970). Given the small amplitude of any orbital velocity variation plus the uncertainties of the velocities, the possible periods cover a broad range from about 4200 to 4950 days, with a best period at 4425 days. This means that our extensive velocity time series (Figure 1), aside from our initial FTS spectrum, covers just 1.4 orbital cycles. With all of our velocities given unit weight, we obtained an orbital solution with the SB1 orbit program (Barker et al. 1967). Because of the broad range of possible periods noted above, we tried starting the values of the orbital period from both the low end and the high end of the 4200–4950 day range. In each case, the orbit program converged to the same set of orbital elements, resulting in a period of 4479 days.

While Galloway et al. (2002) discussed the CfA spectra and velocities for V934 Her, individual velocities were not published. Fortunately, D. Galloway (2017, private communication) provided them to us. To check the compatibility of the zero-points for our velocities and those from CfA, we compared the orbital solution determined from our elements with the CfA velocities. There was good agreement, with the CfA velocities primarily being distributed in the orbit at phases where there was little orbital velocity variation. After comparing the variances of the velocities in the two orbital

solutions, we combined the two data sets, assigning weights of 0.6 to the CfA velocities, and obtained a combined-data solution for the orbital elements. In the combined velocity solution, the orbital period decreased to 4394 days, about a 2σ change. The eccentricity was likewise reduced by about 2σ with the semi-amplitude increased by less than 1σ .

We next looked at the velocity residuals from the combined-data orbital fit. A period search from 100 to 600 days with the program PDFND was carried out on the CfA velocity residuals and resulted in a best period of 406 days, similar to the value found by Galloway et al. (2002). We then made a separate period search of the velocity residuals for our data. A period is clearly present in the data at greater than 10σ in the range 412 ± 10 days. Since both sets of velocities appear to have a second periodicity of about 410 days, our last step was to analyze the two sets of velocities with the general least-squares program of Daniels (1966) to obtain a simultaneous solution for the short- and long-period velocity variations. This final solution resulted in periods of 420.2 ± 0.8 and 4391 ± 33 days, respectively. The uncertainties are 1σ .

Table 1 provides the individual radial velocities for both the CfA and our data. For each observation, the table lists the Heliocentric Julian Date, the observed total velocity, and the observed-minus-calculated velocity residual ($O - C$) to the combined orbit. Also computed and listed in the table are the long-period orbital phase; the long-period velocity, which is equal to the total velocity minus the computed short-period velocity; the short-period orbital phase; and the short-period velocity, which is equal to the total velocity minus the computed long-period velocity. The last column gives the source of the observation. Table 3 provides the orbital elements for both the short- and long-period variations. Although characterized by orbital parameters, the short-period variations, as will be discussed later, result from long secondary period (LSP) velocity changes rather than a third component of the system. The very small value of the long-period orbit mass function, $0.0022 \pm 0.0005 M_{\odot}$, suggests that our 4391 day orbit is seen nearly pole-on. We will return to this point when defining the stellar parameters.

Figure 2 presents the computed velocity curve of the long-period orbit compared with the radial velocities, where zero phase is a time of periastron. Each plotted velocity consists of the total observed velocity minus its calculated short-period velocity. Figure 3 shows the computed velocity curve of the short-period “orbit” compared with the KPNO radial velocities, where zero phase is a time of periastron. Each plotted velocity consists of the total observed velocity minus its calculated long-period velocity.

5. Stellar Parameters

5.1. Photometric Periods

Tomasella et al. (1997) acquired $UBVRI$ photometry on 6 nights over a 2 month period and found no variability at V and B , although the values were a few 0.1 mag different from those previously reported by Garcia et al. (1983). *Hipparcos* found that V934 Her varied by 0.16 mag with a possible period of 31 days. This forms the basis of the General Catalog of Variable Stars SRb designation (Kazarovets et al. 1999). Goranskij et al. (2012), using precision photometry, found periods of 28, 31, and 44 days in V ; 29, 44, and 405 days in B ; and 44 and 415 days in U . Semiregular variables characteristically have simultaneously excited, closely separated periods

Table 2
Spectra Used for Abundance Analysis

ID	Date (UT)	Helio. JD	Spec. Region (Å)	Instrument	Res. (λ/Δλ)	S/N
Ph1	2000 Jul 13	2,451,738.77	15590–15662	Phx/KPNO 2.1	50,000	~100
Ph2	2012 Jun 9	2,456,087.75	15590–15655	Phx/KPNO 2.1	50,000	~100
Ph3	2014 Sep 6	2,456,906.68	15600–15665	Phx/KPNO 4	50,000	~100
Ph4	2003 Apr 20	2,452,749.82	22214–22320	Phx/GS	70,000	~100
Ph5	2012 Jun 8	2,456,086.86	23060–23162	Phx/KPNO 2.1	50,000	~100
FTS	1988 Jul 3	2,447,345.5	20800–24050	KPNO FTS 4	32,000	63
IGRINS	2018 Apr 22	2,458,230.84	15000–17000	IGRINS/GS	45,000	>100
IGRINS	2018 Apr 22	2,458,230.84	20800–24050	IGRINS/GS	45,000	>100

Table 3
Orbital Elements and Related Parameters of V934 Her

Parameter	LSP	Orbit
P (days)	420.17 ± 0.79	4391 ± 33
P (yr)	1.150 ± 0.002	12.02 ± 0.09
T (HJD)	$2,457,894 \pm 22$	$2,457,118 \pm 89$
γ (km s ⁻¹)	...	-47.358 ± 0.063
K (km s ⁻¹)	0.634 ± 0.080	1.915 ± 0.097
e	0.33 ± 0.11	0.354 ± 0.036
ω (deg)	237 ± 23	50.7 ± 8.8
$a \sin i$ (10 ⁶ km)	3.45 ± 0.52	108.2 ± 6.6
$f(m)$ (M_{\odot})	0.0000093 ± 0.0000042	0.00217 ± 0.00047
Standard error of an observation of unit weight (km s ⁻¹)	0.6	0.6

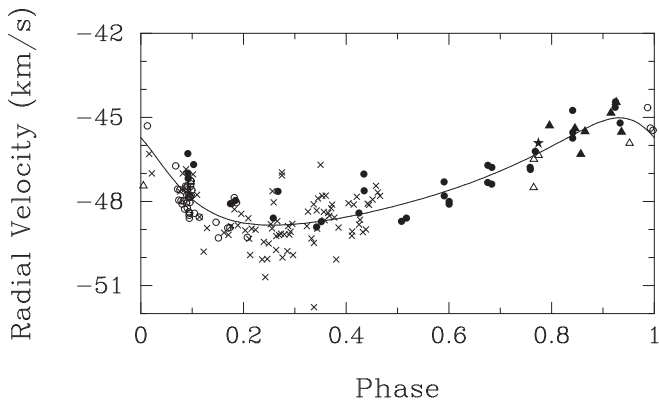


Figure 2. Computed velocity curve of the 4391 day (12.0 yr) long-period orbit compared with our radial velocities and those from CfA. Star = KPNO FTS, filled circles = KPNO coude, open circles = Fairborn Observatory, filled triangles = MSO and KPNO NICMASS, open triangles = KPNO and Gemini South Phoenix, crosses = CfA. Each plotted velocity consists of the total observed velocity minus its calculated short-period velocity. Zero phase is a time of periastron.

from the same overtone (Hartig et al. 2014). The amplitudes in B and V are ~ 0.05 mag, so small as to be easily missed by earlier work. Similarly, Gromadzki et al. (2013) found a period of 44 days.

5.2. The 400 Day Period

A common characteristic of SR variables is an LSP to the dominant pulsation period. The LSP is typically 8–10 times longer than the dominant period (Nicholls et al. 2009; Hartig et al. 2014). Taking the V934 Her photometric period to be

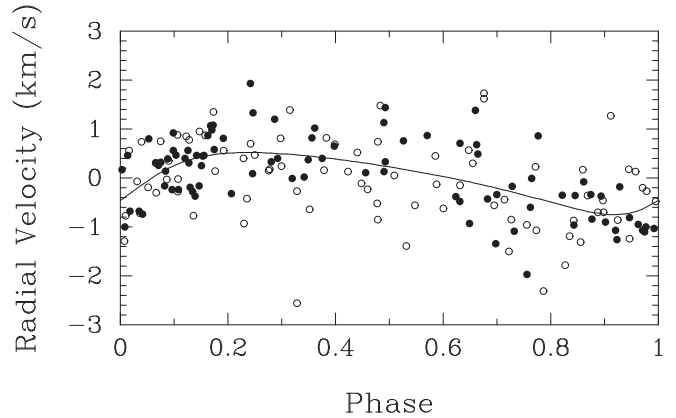


Figure 3. Computed velocity curve of the 420.2 day velocity variation interpreted as an orbit and compared with the velocity residuals. Open circles = CfA velocities; filled circles = our velocities. Each plotted velocity consists of the total observed velocity minus its calculated long-period velocity. Zero phase is a time of periastron.

28–44 days (Goranskij et al. 2012; Gromadzki et al. 2013), the LSP is the ~ 400 day period.

In M giants, LSPs can be detected in both luminosity and velocity variations. As noted above, the first orbit for V934 Her was based on the Galloway et al. (2002) radial velocity period of 404 ± 3 days. If the LSP velocity variations are interpreted as an orbit, the velocity curve is distinctive, with $\omega \sim 250^\circ$ and $e \sim 0.35$ (Hinkle et al. 2002). These parameters are a reasonable match to the “orbital” elements of V934 Her presented by Galloway et al. (2002). As discussed earlier, we have computed a short-period “orbit” with $\omega = 237^\circ$ and $e = 0.33$. We also note the similarity of these numbers to the LSP “orbit,” $\omega = 229.5^\circ$ and $e = 0.33$, of the very well-studied SySt CH Cyg (Hinkle et al. 2009).

Because the orientation of the star is known, V934 Her presents an interesting case of LSP. Assuming that the rotation axis of the M giant is parallel to that of the orbit, the star is seen nearly pole-on. In this case, models for the LSP that require semidetached binaries (Wood et al. 1999; Soszyński 2007) and rotating spots with dust formation (Takayama et al. 2015) can be excluded. As discussed by Stothers (2010) and Saio et al. (2015), this narrows the explanations to pulsation mechanisms involving convection. A global pulsation mechanism for LSP now appears to be widely accepted if not fully understood (Trabucchi et al. 2017).

The LSPs are associated with increased mid-IR excess (Wood & Nicholls 2009). In the case of V934 Her, this is in agreement with the results of Masetti et al. (2002), who found a

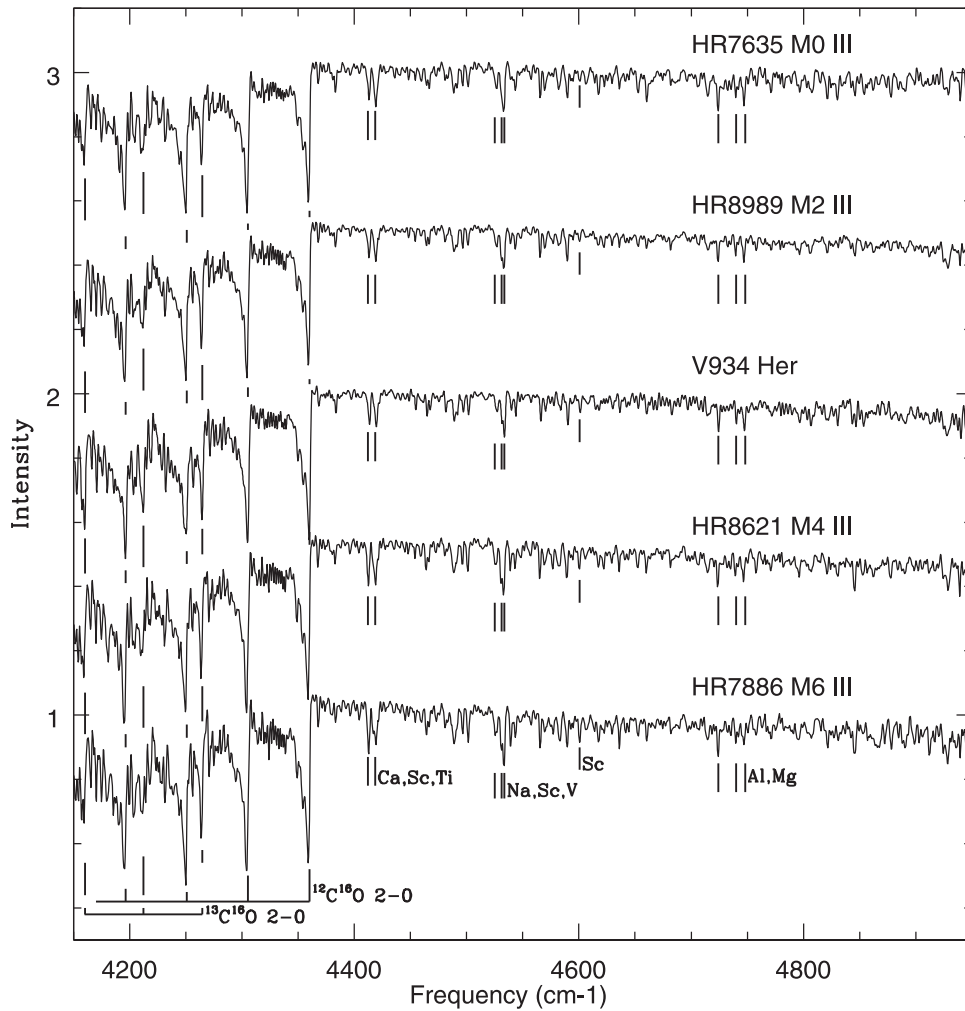


Figure 4. FTS spectra in the K -band at $R \sim 3000$ comparing the spectrum of V934 Her to M0 III through M6 III standard star spectra from Wallace & Hinkle (1997).

larger-than-expected IR excess. Masetti et al. (2002) reported a tentative period of ~ 400 days from *RXTE* ASM observations. Galloway et al. (2002) analyzed the same data extended by an additional year and refined this as a period of 404 ± 20 days. The existence of the LSP in the X-ray data would link the LSP to cyclic enhancements of mass loss from the M III. Corbet et al. (2008) analyzed Swift BAT observations and *RXTE* ASM observations, including data previously analyzed by Masetti et al. (2002) and Galloway et al. (2002), but was not able to find the ~ 400 day period.

5.3. Temperature, Luminosity, and Surface Gravity

Garcia et al. (1983) found that V934 Her had an optical spectral type of M3 II, while Masetti et al. (2002) determined an optical spectral type of M2 III, which was confirmed by Goranskij et al. (2012). Their photometry of V934 Her does not show any measurable reddening. While Gaudenzi & Polcaro (1999) claimed that the spectrum is abnormal, this has been refuted (see, for instance, Masetti et al. 2002). Other than the claim of Gaudenzi & Polcaro (1999), there is no evidence for spectral variability. Tomasella et al. (1997) were not able to detect changes in the optical spectrum of V934 Her during a strong X-ray outburst.

The FTS spectrum of V934 Her discussed earlier covers the $2.0\text{--}2.5 \mu\text{m}$ near-IR K band. After apodizing to $R \sim 3000$, this

spectrum was compared (Figure 4) to M-giant standards from Wallace & Hinkle (1997). The strong CO features mark V934 Her as a luminous star. For the mid-M temperature classes, a good indicator of temperature is the Sc I 4600 cm^{-1} line. In V934 Her, this line is approximately intermediate in strength between the M2 III and M4 III spectra. Other atomic features are also stronger than in the M2 spectrum. We assign a temperature classification of M3. Importantly, the infrared spectrum of V934 Her looks like that of a normal star with no emission features in its K -band spectrum.

The distance to V934 Her has been discussed by both Garcia et al. (1983) and Masetti et al. (2002), with their results differing by a factor of two. This discrepancy has been resolved by the *Gaia* parallax of 1.837 ± 0.032 mas, i.e., a distance of 544^{+10}_{-9} pc (Gaia Collaboration et al. 2018). Combining the distance with the galactic coordinates, V934 Her is 296 pc above the galactic plane. Goranskij et al. (2012) suggested that V934 Her is unreddened. Confirmation is provided by the images of Schlafly & Finkbeiner (2011), who found that $E(B - V)$ is at most 0.038. Ignoring reddening, the 2MASS (Cutri et al. 2003) $m_K = 2.988$ mag results in an absolute K magnitude $M_K = -5.690$ mag. Taking $J - K = 1.181$ mag, the 2MASS color of V934 Her, the K -band bolometric correction from Bessell & Wood (1984) is 2.92 mag. The resulting bolometric magnitude for V934 Her is -2.775 mag, corresponding to $1028 \pm 40 L_{\odot}$, where the formal uncertainty

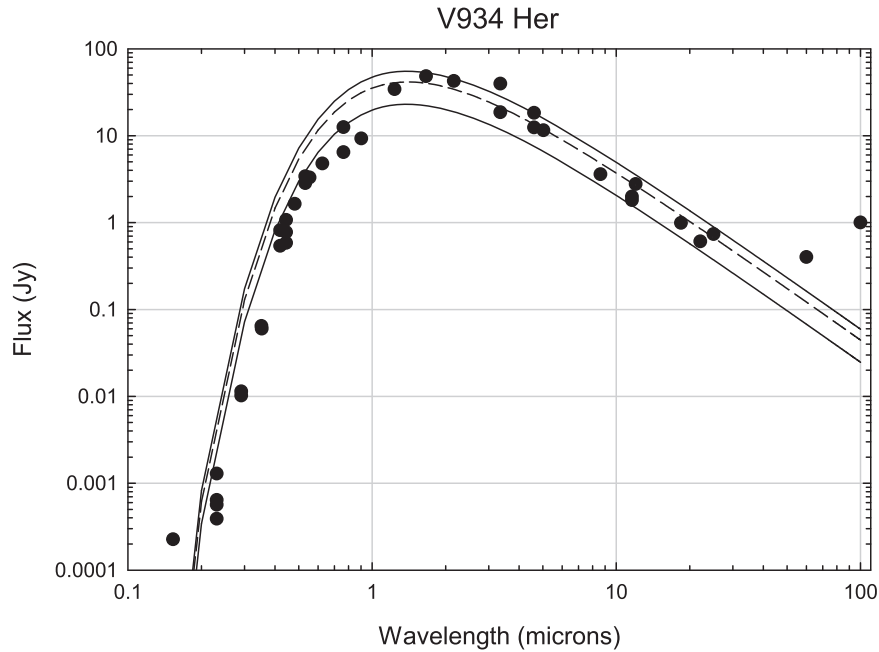


Figure 5. Photometry of V934 Her/4U 1700+24 from the literature compared to a 3650 K blackbody. The dashed line is a best fit, while the two solid lines correspond to high and low envelopes. The blackbody integrated flux is $1.4 \times 10^{-10} \text{ W m}^{-2}$. Assuming the *Gaia* distance of 544 pc, the bolometric magnitude is -3.1 . The blackbodies (lower to upper fits) correspond to stellar radii of 70, 91, and $105 R_{\odot}$. The blackbody fit shows IR excess suggesting a modest mass-loss rate and UV excess due to the NS.

is from the distance. The uncertainties associated with the infrared photometry and bolometric correction are not available.

Van Belle et al. (1999) gave an effective temperature for an M3 III of 3573 ± 22 K. Alternately, using the $V - K$ color of V934 Her, the $V - K$ color- T_{eff} relation of van Belle et al. (1999) yields 3677 K. Dyck et al. (1996) suggested an effective temperature for an M3 III of 3650 K. Adopting a 3650 K effective temperature as a mean value, the literature photometry for V934 Her/4U 1700+24 is shown in Figure 5, fit with a 3650 K blackbody. The blackbody integrated flux is $1.4 \pm 0.1 \times 10^{-10} \text{ W m}^{-2}$. Correcting for the *Gaia* distance of 544 pc, the bolometric magnitude is -3.1 ± 0.1 , i.e., $L = 1367 \pm 120 L_{\odot}$.

We adopt mean values for the temperature and luminosity with uncertainties embracing the range of values, $L = 1200 \pm 200 L_{\odot}$ and $T_{\text{eff}} = 3650 \pm 100$ K. The values for the temperature and luminosity are in good agreement with both the observational Hertzsprung-Russell Diagram and the evolutionary tracks for an M3 III resulting from a low-mass progenitor (Escorza et al. 2017). Similarly, using the *Gaia* distance, K_S , and $J - K$ colors, the relations of Lebzelter et al. (2018) confirm that V934 Her is on either the red giant branch (RGB) or faint asymptotic giant branch (AGB).

We have argued that the ~ 410 day period of V934 Her is not an orbital period but a pulsational LSP. The period-luminosity relation of Wood (2000) can be applied to the photometric periods. Goranskij et al. (2012) and Gromadzki et al. (2013) found periods of 28 and 44 days with an LSP of 410 days. The LSP is associated with a primary period on the first-overtone B sequence (Wood et al. 1999; Trabucchi et al. 2017). We assume that the 44 day period is the first-overtone B-sequence period and the 28 day period is the second-overtone A-sequence period. From the midline of the relations for the 28, 44, and 410 day periods, the corresponding Large Magellanic Cloud (LMC) W_{JK} from Figure 1 of Trabucchi et al. (2017) or Figure 2 of Soszyński et al. (2007) is

11.37. Assuming a distance modulus of $m - M = 18.5$ mag for the LMC, this corresponds to $M_K = -6.3$, 0.6 mag brighter than measured. However, the $P - L$ relations have a width > 0.5 mag in W_{JK} , so the $P - L$ bolometric magnitude is in agreement with the absolute K mag determined from the *Gaia* distance.

The blackbody fit to the photometry yields the stellar radius, as well as the flux. The uniformly illuminated radius required for the blackbody is $91^{+14}_{-21} R_{\odot}$. The Bourgués et al. (2014) database gives a limb-darkened angular diameter computed from the colors of V934 Her of $2R = 1.544 \pm 0.121$ mas. Using the *Gaia* distance, the red giant radius is $90 R_{\odot}$. Van Belle et al. (1999) gave a smaller radius of $71 R_{\odot}$, but the relationship has considerable width.

5.4. Mass

From the models of Charbonnel et al. (1996), the luminosity of $1200 L_{\odot}$ and T_{eff} of 3650 K place V934 Her on the early AGB of a solar-metallicity $1.7 M_{\odot}$ star. STAREVOL tracks by Escorza et al. (2017) suggest a mass a few $0.1 M_{\odot}$ smaller. The NS companion in the V934 Her system has a limited range of mass. The upper limit to the mass of an NS occurs at $\sim 3 M_{\odot}$, when the internal sound speed reaches the speed of light. Such a large mass for the NS seems unlikely. Masses of NSs in binary radio-pulsar systems are all very close to $1.35 M_{\odot}$ (Thorsett & Chakrabarty 1999). Masses larger than $1.35 M_{\odot}$ might occur (Lorimer & McLaughlin 2006), but masses measured for LMXB NSs, which can be uncertain, seldom exceed $1.5 M_{\odot}$ (Casares et al. 2017).

The mass function from the orbit of the M giant is

$$f(m) = M_{\text{NS}}^3 \sin^3(i) / (M_{\text{RG}} + M_{\text{NS}})^2 = 0.0022.$$

If we assume that $M_{\text{NS}} = 1.35 M_{\odot}$ and $M_{\text{RG}} = 1.7 M_{\odot}$, the orbital inclination is 11.7° . Lower masses for the red giant from different evolution models or mass loss drive the inclination

Table 4
Parameters of the V934 Her M III

Parameter	Value	Source
Distance	544 ± 10 pc	<i>Gaia</i>
Spec. type	M3 III	Figure 3; T_{eff} and luminosity
T_{eff}	3650 ± 100 K	Sp. Ty.; $V - K$; CO T_{exc}
Luminosity	$1200 \pm 200 L_{\odot}$	See text; Figure 4
Radius	$90 \pm 20 R_{\odot}$	Figure 4; van Belle et al. (1999)
Mass	$1.6^{+0.1}_{-0.2} M_{\odot}$	Evol. tracks and mass loss
Surface gravity ($\log g$)	0.7 ± 0.2 (cm s^{-1})	Mass and radius
Inclination ^a	$11^{\circ}3 \pm 0^{\circ}4$	Assume equator and orbit coplanar
[Fe/H]	-0.60 ± 0.10	See text
[α /H]	-0.33 ± 0.12	See text (Mg+Si+Ca)
Age	~ 2 Gyr	Evol. tracks

Note.

^a Equator to plane of sky.

smaller. If, as suggested by Lü et al. (2012), the NS has accreted mass from the giant, the inclination is also smaller. For example, an M-giant mass of $1.4 M_{\odot}$ reduces the inclination to $10^{\circ}9$. We conclude that an orbital inclination in the range of $11^{\circ}3 \pm 0^{\circ}4$ is in agreement with the mass estimates. The probability of an inclination of $11^{\circ}7$ or less is 2%.

If we adopt a mass for the M giant of $1.6 M_{\odot}$, averaged between the evolutionary models, and a radius of $90 R_{\odot}$, then the surface gravity is 5.4 cm s^{-1} , $\log g = 0.7$, with the uncertainty in the mass and radius resulting in a uncertainty in $\log g$ of ~ 0.2 . The parameters for the M giant are presented in Table 4. For abundance determinations (Section 6), we have adopted atmospheric models within the grid of model atmospheres of $T_{\text{eff}} = 3650$ K and $\log g = 0.5$.

6. Abundances

6.1. Methods

Abundances were measured with the spectral synthesis technique in the classical way, i.e., employing local thermodynamic equilibrium analysis based on 1D hydrostatic model atmospheres (MARCS; Gustafsson et al. 2008). Synthetic spectra were calculated with the code developed by M. Schmidt (WIDMO; Schmidt et al. 2006). The general characteristics of the adopted method, together with its justification, are discussed in a series of papers on chemical composition analysis in SySt giants (Gałan et al. 2016 and references therein). In summary, the abundance calculations for given model atmospheres were performed as follows. The initial-starting values for the free parameters were obtained by adjusting roughly by eye the synthetic to observed spectrum through several iterations. Next, the simplex algorithm (Brandt 1998) was used for χ^2 minimization in the parameter space. Besides the relevant abundances and isotopic ratios, additional free parameters were the line broadening for each spectrum expressed as a macroturbulent velocity, ζ_t , and a microturbulent velocity, ξ_t . For the V934 Her analysis, ξ_t was found by examining the large range of excitation potentials and line strengths, especially from $^{12}\text{C}^{16}\text{O}$ lines over the broad wavelength range of the IGRINS spectrum.

The excitation potentials and gf values for transitions in the case of atomic lines in the narrow H -band region of the Phoenix spectra were taken from the list by Mélendez & Barbuy (1999) and for the K -band region from the Vienna Atomic Line Database (Kupka et al. 1999). For the molecular data in the K -band region, we used line lists by Goorvitch (1994) for CO, R. L. Kurucz⁶ for OH, and Sneden et al. (2014) for CN. For the H -band IGRINS spectrum, we used the DR12 release of the APOGEE line lists (Shetrone et al. 2015).

The spectrum synthesis was run with model stellar atmospheres covering a broad range of effective temperature from 2900 to 4250 K, surface gravity from 0.0 to +1.0, and metallicity from -0.5 to 0.0. The data sets were fit separately, since the data covered a range of resolution and S/N. The regions of the spectra contaminated with artifacts or insufficiently well-reduced telluric absorption features were excluded from the analysis.

6.2. Limitations of the Model Atmosphere

The parameters derived above for V934 Her, $T_{\text{eff}} = 3650$ K, $\log g = +0.5$, and approximate solar metallicity, resulted in synthetic spectra that were excellent fits to the H -band spectra (Figure 6). However, to our surprise, the strong lines in the K -band region were best fit with a significantly lower effective temperature, $T_{\text{eff}} = 3100$ K (FTS spectrum) and $T_{\text{eff}} = 3000$ K (IGRINS spectrum). The surface gravity remained $\log g = 0.5$ in all cases. The best example of the poor fit by the 3650 K synthetic spectrum is for the CO first overtone, where lines of different excitation potentials and strengths are present (Figure 7). The IGRINS spectra are especially interesting, since the first- and second-overtone CO regions were observed simultaneously. The H -band second-overtone CO lines are fit by $T_{\text{eff}} = 3650$ K, while the first-overtone CO lines in the K -band region appear to require an ~ 600 K lower temperature.

As noted, IGRINS K and H spectra were taken simultaneously; hence, explanations for the lower excitation temperatures that invoke time variability can be ruled out. Since weak lines are fit by a 3650 K effective temperature while strong lines are not, the outer layers of the model atmosphere must be too hot. To further investigate this problem, we did a curve-of-growth analysis of the CO lines. This technique, discussed by Hinkle et al. (2016), requires large spectral coverage, which was made possible by our IGRINS observation. Using the CO second-overtone lines, we found a CO excitation temperature of 3375 K. The CO second-overtone lines are generally weak, at most $\sim 30\%$ deep. Comparison to a similar analysis of spectral standard M giants shows that a 3375 K excitation temperature corresponds to an effective temperature of ~ 3650 K. This provides further confirmation that the spectral type has been correctly assigned. On the other hand, the strong CO first-overtone lines have a much lower excitation temperature. The relatively small sample of strong lines does not allow a solution, but the excitation temperature is less than 3000 K.

The K -band region of the V934 Her spectrum contains measurable lines from the CO isotopologues $^{13}\text{C}^{16}\text{O}$ and $^{12}\text{C}^{18}\text{O}$. These lines are not nearly as strong as the $^{12}\text{C}^{16}\text{O}$ 2–0 lines. There are also clear upper limits for the 2–0 $^{12}\text{C}^{17}\text{O}$ lines. With $T_{\text{exc}} = 3375$ K, curves of growth were computed for the isotopologues. Shifts between these curves of growth give the

⁶ <http://kurucz.harvard.edu>

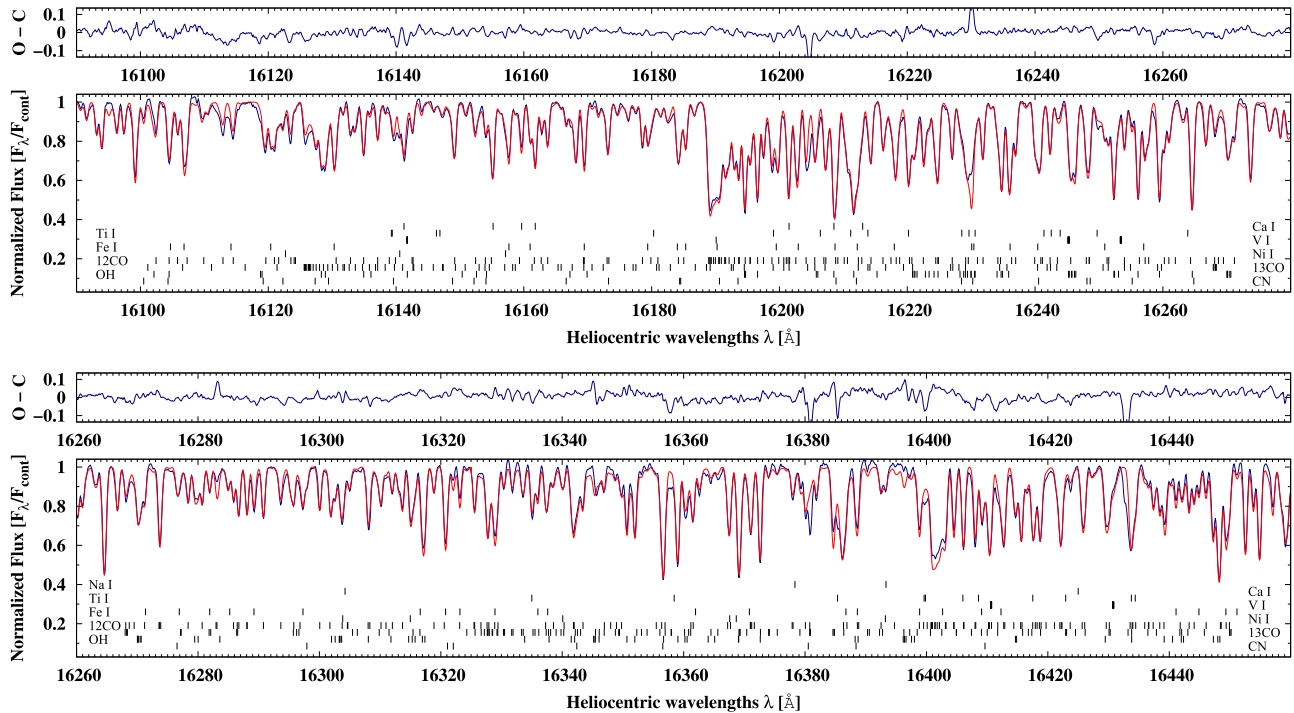


Figure 6. IGRINS H -band spectrum (blue line) shown as normalized flux as a function of wavelength in \AA in the region 16100–16440 \AA compared to the synthetic spectrum (red line) calculated with the final abundances (Table 5). Individual lines are identified with dashes below the spectrum. The $^{12}\text{C}^{16}\text{O}$ 6–3 band head is at 16190 \AA , and the $^{12}\text{C}^{16}\text{O}$ 7–4 band head is at 16400 \AA . Residuals ($O - C$) to the fit are shown in the box above the spectrum.

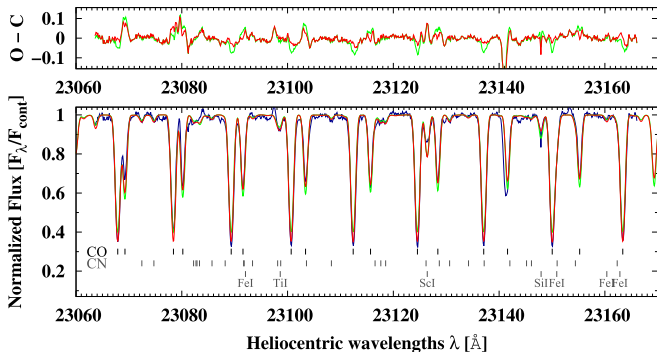


Figure 7. Lower panel: Phoenix spectrum of V934 Her observed 2012 June 8 (blue line) compared to synthetic spectra obtained with two different adopted effective temperatures, $T_{\text{eff}} = 3100$ K (red line) and 3600 K (green line). The spectrum is dominated by strong CO bands superimposed on a background of weak CN and atomic lines. The hotter atmosphere does not give a good fit to the alternating high- and low-excitation 2–0 $^{12}\text{C}^{16}\text{O}$ lines. Dashes below the spectrum and the upper panel are the same as in Figure 6.

isotopic abundances (Figure 8). We find $^{12}\text{C}/^{13}\text{C} = 10 \pm 4$, $^{16}\text{O}/^{17}\text{O} = 2500_{-1000}^{+1500}$, and $^{16}\text{O}/^{18}\text{O} = 262 \pm 100$. These values match the values found from the spectrum synthesis. The curve-of-growth analysis compares weak second-overtone H -band $^{12}\text{C}^{16}\text{O}$ with similar-strength isotopic lines in the K band. Spectrum synthesis uses a model atmosphere to fit a spectral interval. The failure of the synthetic spectrum to fit the strong lines must not be a problem related to wavelength, since the model works for both H and K weak lines. We also measured the CO lines in the K -band FTS spectrum. The equivalent widths from the FTS and IGRINS spectra are in reasonable agreement, again demonstrating that there is no time-dependent problem.

Tsuji (1988) reported similar difficulties in fitting the CO first-overtone lines. Tsuji found that extra absorption in low-excitation first-overtone CO lines is a common property of late-type spectra. He attributed the low-temperature absorption to a quasi-static, turbulent, 1000–2000 K extended region in the outer atmospheres of these stars.

Chakrabarty & Roche (1997) suggested that the NS in the SyXB V2116 Oph system heats the red giant, altering the TiO band strengths and impacting estimates of the spectral class based on this molecule. The orbit of V2116 Oph is close to edge-on. Chakrabarty & Roche (1997) derived a mean spectral class of M5. In our analysis of V2116 Oph (Hinkle et al. 2006), we found that the M5 III effective temperature, $T_{\text{eff}} = 3400$ K, agreed with the effective temperature determined from spectral synthesis of the infrared spectrum. This analysis was based on Phoenix spectra covering small regions of the spectrum. In 2018 April, we observed V2116 Oph with IGRINS. Using this observation, we obtained $T_{\text{exc}} = 3200$ K for the CO second overtone. This corresponds to $T_{\text{eff}} = 3370$ K, so it is in good agreement with the Chakrabarty & Roche (1997) spectral type. The separation of the NS and M giant in V934 Her is about two times larger than it is in V2116 Oph, so NS heating should be even less in V934 Her.

6.3. Abundance Results

Table 5 lists the final values of the abundances obtained from the spectra for $T_{\text{eff}} = 3650$ K and $\log g = 0.5$. Resulting values for the broadening parameters are presented in Table 6. The contributions to the uncertainties in the abundances are given in Table 7. Uncertainties in the abundances come mainly from uncertainties in stellar parameters. The final uncertainty in Table 7 is the quadrature sum

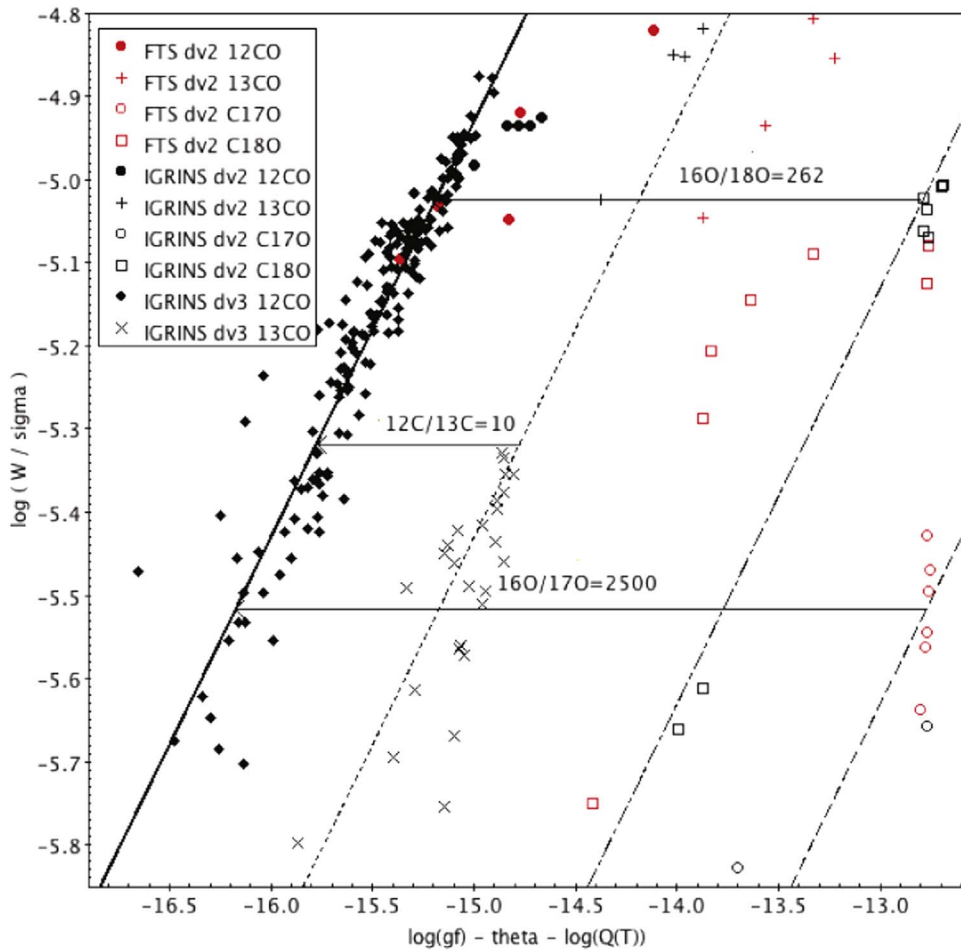


Figure 8. Curves of growth for the weak CO isotopologue lines in V934 Her. Measurements from the IGRINS and FTS spectra are shown separately. The IGRINS spectrum has a much higher S/N. The IGRINS spectrum covers the CO $\Delta v = 3$ and 2 regions, while the FTS spectrum only covers the CO $\Delta v = 2$ region. The $\Delta v = 3$ lines from the rare isotopologues were not detected. The shifts between the curves of growth give the isotopic ratios (labeled).

of the uncertainties of each model parameter. The IGRINS results derived entirely from the H band are similar to the FTS and Phoenix results from the K band. In spite of the difficulties in fitting the spectra with a consistent model atmosphere, the K - and H -band results (Table 5) are similar, with the exception of the N abundance derived from the FTS spectrum. We attribute this to the lower quality of that spectrum. However, to err on the side of caution, in the subsequent discussion, we use only the H -band results, with the exception of the C and O isotopes.

7. Discussion

7.1. Stellar Evolution

The probability of forming a binary system outside of a globular cluster by gravitational capture is nearly zero. Stellar evolutionary tracks show that the main-sequence mass of the V934 Her giant was in the range ~ 1.4 – $1.7 M_{\odot}$, so the unevolved system was a binary consisting of the massive progenitor of the NS and an $\sim 1.6 M_{\odot}$ companion. The $^{16}\text{O}/^{17}\text{O}$ oxygen isotope ratio is very large, ≥ 2000 . This large value indicates that the ZAMS mass of the M-giant progenitor was low, $\lesssim 1.5 M_{\odot}$ (Smith 1990; Hinkle et al. 2016). The agreement of masses from the evolutionary tracks and abundances requires that mass transfer from the proto-SN supergiant to the current M giant, if any, is no more than a few $0.1 M_{\odot}$. The main-sequence lifetime for a $1.6 M_{\odot}$ star is ~ 2 Gyr

(Charbonnel et al. 1996), while the lifetime of a $> 8 M_{\odot}$ star is $\lesssim 100$ Myr (Vassiliadis & Wood 1993; Tauris & van den Heuvel 2006). Thus, the age of the NS is ~ 2 Gyr.

The carbon ^{12}C and nitrogen ^{14}N abundances of the M III (Table 5) reflect mixing during the first dredge-up. This is confirmed by the low carbon isotope ratio, $^{12}\text{C}/^{13}\text{C} \sim 7$ – 11 , and is consistent with a red giant or early AGB status for the M III. The giant in V934 Her has a slightly subsolar metallicity. Following Lambert (1987), we have computed $[\alpha/\text{Fe}] = +0.27$ from the average of the Mg, Si, and Ca abundances. The $[\alpha/\text{Fe}]$ versus $[\text{Fe}/\text{H}]$ is close to the mean relation (Lambert 1987) and shows no notable peculiarity for this star. The α -element and Fe abundances are similar to the abundances of many other SySt giants (Gafan et al. 2016, 2017). Casares et al. (2017) reported that in LMXBs, many of the low-mass stars show enhancements of Fe and α elements. Modeling suggests that this results from the capture of SN ejecta by the dwarf companion. We conclude that in the SyXB giants, any SN ejecta on the surface has been mixed into the interior as the star evolved up the giant branch.

Lü et al. (2012) discussed Monte Carlo simulations of the SyXB population, including CCSs, electron-capture SNe (ECSs), and AIC. Their study concludes that between 70% and 98% of SyXB NSs are formed via core collapse, with the remainder formed via ECSs. The simulation finds that systems forming via ECSs have short initial periods and have passed

Table 5
Abundance Summary

Element	FTS		Phoenix		IGRINS ^a	
	$\log \epsilon(X)^b$	[X] ^c	$\log \epsilon(X)^b$	[X] ^c	$\log \epsilon(X)^b$	[X] ^c
C	7.79 ± 0.05	-0.64 ± 0.10	7.91 ± 0.03	-0.52 ± 0.08	7.84 ± 0.01	-0.59 ± 0.06
N	8.23 ± 0.11	+0.40 ± 0.16	7.69 ± 0.06	-0.14 ± 0.11	7.63 ± 0.03	-0.20 ± 0.08
O	8.27 ± 0.07	-0.42 ± 0.12	8.35 ± 0.03	-0.34 ± 0.08	8.29 ± 0.01	-0.40 ± 0.06
Na	5.72 ± 0.21	-0.49 ± 0.25	5.44 ± 0.11	-0.77 ± 0.15
Mg	7.35 ± 0.03	-0.24 ± 0.07
Al	6.45 ± 0.18	+0.02 ± 0.22	6.08 ± 0.08	-0.35 ± 0.12
Si	7.71 ± 0.13	+0.20 ± 0.16	7.23 ± 0.05	-0.28 ± 0.08
S	7.10 ± 0.27	-0.02 ± 0.30
K	4.75 ± 0.08	-0.29 ± 0.13
Ca	6.07 ± 0.13	-0.25 ± 0.16	5.84 ± 0.05	-0.48 ± 0.08
Sc	3.17 ± 0.10	+0.01 ± 0.14	2.96 ± 0.21	-0.20 ± 0.25
Ti	4.76 ± 0.11	-0.17 ± 0.15	4.52 ± 0.15	-0.41 ± 0.19	4.43 ± 0.06	-0.50 ± 0.10
V	3.32 ± 0.11	-0.57 ± 0.19
Cr	4.94 ± 0.07	-0.68 ± 0.11
Mn	4.84 ± 0.11	-0.58 ± 0.15
Fe	7.03 ± 0.08	-0.44 ± 0.12	6.93 ± 0.07	-0.54 ± 0.11	6.87 ± 0.01	-0.60 ± 0.05
Co	4.37 ± 0.05	-0.56 ± 0.10
Ni	6.50 ± 0.29	+0.30 ± 0.33	5.85 ± 0.15	-0.35 ± 0.19	5.66 ± 0.08	-0.54 ± 0.12
¹² C/ ¹³ C	6.7 ± 0.9	10.2 ± 0.3	...
¹⁶ O/ ¹⁷ O	4500 ± 700	2750 ± 320 ^d	...
¹⁶ O/ ¹⁸ O	390 ± 90	250 ± 30 ^d	...

Notes.^a From *H*-band spectrum.^b $\log \epsilon(X) = \log(N(X)N(H)^{-1}) + 12.0$. Uncertainty is 3σ from the fit. See Table 7 for the total uncertainty. Abundances in dex.^c Relative to the Sun [X] abundances in respect to the solar composition of Asplund et al. (2009); Scott et al. (2015a, 2015b).^d From *K*-band spectrum.**Table 6**
Line-broadening Parameters

Spectrum	ζ_t (km s ⁻¹)	ξ_t (km s ⁻¹)
FTS	5.84 ± 0.74	2.49 ± 0.09
Ph1	3.65 ± 0.65	2.47 ± 0.12
Ph2	4.49 ± 0.59	2.47 ± 0.12
Ph3	4.16 ± 0.51	2.47 ± 0.12
Ph4	6.67 ± 0.35	2.47 ± 0.12
Ph5	5.14 ± 0.52	2.47 ± 0.12
IGRINS	5.41 ± 0.34	2.31 ± 0.07

through a common-envelope phase. Similar scenarios are discussed by Willems & Kolb (2002).

The simulated SyXB population of Lü et al. (2012) has typical parameters similar to those of V934 Her. Perhaps the existence of binary systems that survived a CCS should not be surprising, since all massive stars have at least one companion (Duchêne & Kraus 2013), and the number of binary survivors of an SN is very small. In the case of V934 Her, the *Gaia* proper motions of -10.06 ± 0.04 mas yr⁻¹ in R.A. and -6.40 ± 0.05 mas yr⁻¹ in decl. correspond to velocities of -25.9 and -16.5 km s⁻¹ at the *Gaia* distance of 544 pc. The γ velocity for the binary is -47.36 ± 0.06 km s⁻¹, so the space velocity of this star is not unusually large.

Assuming an NS mass of $1.35 M_\odot$, a mass of $1.6 M_\odot$ for the M giant, and an orbital period of 12.0 yr, Kepler's third law gives a semimajor axis a of 7.52 au for V934 Her. At periastron, the separation is $a(1 - e) = 4.86$ au. From the formula of Eggleton (1983), the M-giant Roche lobe at periastron is 1.93 au or $415 R_\odot$, which is much larger than the current stellar radius of $\sim 90 R_\odot$.

Table 7
Abundance Uncertainty Summary^a

Element	$\Delta T_{\text{eff}} = +100$ K	$\Delta \log g = +0.5$	$\Delta \xi_t = +0.1$	Δ^b
C	+0.04	+0.19	0.00	±0.20
N	+0.05	-0.06	+0.01	±0.08
O	+0.12	+0.03	-0.01	±0.13
Na	+0.13	-0.20	-0.02	±0.24
Mg	+0.03	-0.09	+0.03	±0.10
Al	+0.06	-0.03	-0.03	±0.08
Si	-0.04	+0.11	+0.02	±0.12
K	+0.03	+0.04	-0.01	±0.06
Ca	+0.05	+0.03	-0.01	±0.06
Ti	+0.07	+0.09	-0.02	±0.12
V	+0.07	+0.09	-0.02	±0.12
Cr	+0.05	+0.05	-0.01	±0.08
Mn	-0.01	+0.09	0.00	±0.10
Fe	-0.02	+0.09	-0.01	±0.10
Co	+0.01	+0.12	+0.01	±0.13
Ni	-0.02	+0.11	0.00	±0.12

Notes.^a *H*-band IGRINS data and model atmospheres with parameters $T_{\text{eff}} = 3600$ K, $\log g = 0.5$, and $\xi_t = +2.3$.^b $[(\Delta T_{\text{eff}})^2 + (\Delta \log g)^2 + (\Delta \xi_t)^2]^{0.5}$.

When the current M giant evolves to a tip AGB star its stellar radius will increase to $\sim 250 R_\odot$ (Ohnaka et al. 2006). At the same time, the mass-loss rate will increase from the current $\sim 10^{-9} M_\odot \text{yr}^{-1}$ to $\sim 10^{-6} M_\odot \text{yr}^{-1}$. Over the 10^6 yr thermally pulsing (TP) AGB lifetime (Vassiliadis & Wood 1993), the current $1.6 M_\odot$ M III will lose $\sim 1 M_\odot$ to become a $0.6 M_\odot$ white

dwarf (Si et al. 2018). As the mass loss increases, mass transfer to the NS will decrease the orbital separation. Simulations by Wiktorowicz et al. (2017) predict the evolution of ultraluminous X-ray sources from NS–low-mass star binaries with masses nearly identical to those in the V934 Her system. A complicating factor is the increased absorption of the X-ray flux due to the 10^3 increase in mass loss.⁷

7.2. Orbital Evolution

From radial velocity observations, Famaey et al. (2009) obtained orbits for nonsymbiotic M-giant stars in the *Hipparcos* survey and combined the results with M-giant orbits from the literature to produce a sample of 29 systems. In a follow-up paper, Jorissen et al. (2009) examined the (e – $\log P$) diagram of those 29 M-giant binaries from Famaey et al. (2009). Although V934 Her has a degenerate companion, it has an unremarkable optical spectrum. Thus, we compare V934 Her with the M-giant sample of Famaey et al. (2009).

Figure 1 of Jorissen et al. (2009) shows that M giants with periods up to about 1500 days all have eccentricities below 0.25. For M giants with longer-period orbits, except for one nearly circular orbit system, the eccentricities range from about 0.3 to 0.75. With its period of 4391 days and eccentricity of 0.35, V934 Her clearly has a very noncircular orbit but is situated near the lower end of the eccentricity distribution. The kick velocity resulting from asymmetry during a CCS can be substantial to the point of disrupting the binary (Lyne & Lorimer 1994). Given the large, 4.8 au, periastron separation for V934 Her, tidal forces have not substantially acted to circularize the orbit. The eccentricity near the lower bound of M giants may well reflect the primordial eccentricity of the system and apparently was not significantly increased as a result of the SN event. This suggests that the NS resulted from an ECS that has a low kick velocity (Lü et al. 2012).

7.3. LSP

The presence of an LSP pulsation of the M giant is supported by both spectroscopy and photometry. The 420 day spectroscopic “orbit” is a close match to the velocity variations observed in other LSP variables (Hinkle et al. 2002). The luminosity derived from *Gaia* places the 44 day photometric period of V934 Her on the AGB pulsation first overtone, the 28 day period on the second overtone, and the 404 day photometric period on the LSP sequence (Trabucchi et al. 2017). Assuming the stellar equator is aligned with the plane of the orbit, the M giant is seen nearly pole-on. This narrows the list of possible LSP mechanisms to those favoring convection (Trabucchi et al. 2017). Strong absorption lines in the M-giant spectrum are not well fit by a standard model atmosphere. A connection between the atmospheric structure and LSP is an area for future investigation.

Published observations show a tentative connection between the LSP and X-ray activity, presumably driven by changes in the mass loss. In the SyXB/SySt system V2116 Oph/GX 1+4, activity is enhanced near periastron passage (Ikiewicz et al. 2017). Although the V934 Her orbit is significantly more eccentric than that of V2116 Oph, the periastron separation, 2.28 au, is still about twice that of V2116 Oph/GX 1+4. It would be interesting to confirm the connection between LSP

and X-ray activity and see if the activity of V934 Her also increases near periastron.

8. Conclusions

The NS–M giant symbiotic binary V934 Her is shown to have a 12 yr orbit with an eccentricity of 0.35. The period previously found in the velocity data, 404 days and revised here to 420 days, is not the binary orbit but the LSP pulsation of the M giant. We find the M giant to have a spectral type of M3 III and slightly subsolar abundances. The $^{16}\text{O}/^{17}\text{O}$ is consistent with a progenitor main-sequence star having a mass similar to that determined from the observed stellar parameters and evolutionary tracks. As is the case for the SyXB star V2116 Oph, the elemental abundances do not show any peculiarities that would reveal the details of either a previous common-envelope stage with the proto-NS massive star or of mass that was transferred during the SN event. The velocity and orbit of V934 Her also appear to be little affected by the SN, suggesting that it was an ECS.

The main-sequence lifetime of the M-giant progenitor was ~ 2 Gyr. The NS evolved from a massive star in Myr, so the NS is nearly 2 Gyr old. Two other SyXBs are known to be old, 4U 1954+319 (Enoto et al. 2014) and V2116 Oph/GX 1+4 (Hinkle et al. 2006). Ages of Gyr for the SyXBs are similar to ages derived for the NS in some of the standard LMXBs (Wijnands & van der Klis 1998). The observed NS properties are driven by mass accretion from the M-giant stellar wind. In the case of V934 Her/4U 1700+24, neither X-ray nor radio pulsations have been detected from the NS component, but all evidence suggests that this binary system is seen nearly pole-on.

We have compared the properties of the V934 Her M giant to those of the M giant in the SyXB binary V2116 Oph. Both are of similar luminosity, and both appear to be on the giant branch or early AGB. It seems likely that V2116 Oph is the most X-ray luminous of the SyXBs because of higher mass loss from its cooler M5/6 giant combined with a relatively short (for an SyXB) 3.18 yr orbital period. The separation between the components in the V2116 Oph system is about half that of the V934 Her system. The only two members of the SyXB group with determined orbits are V2116 Oph and V934 Her. The lack of optical emission lines in the M-giant spectra and the ultralong NS pulse periods in other SyXBs strongly suggest that these systems are similar to V934 Her with long orbital periods.

We are indebted to Duncan Galloway for sending his archival radial velocity observations of V934 Her. We thank Sharon Hunt for providing several references critical to this project. The FTS spectrum was observed by Verne Smith. We thank him for bringing the existence of this spectrum to our attention.

This research was facilitated by the SIMBAD database, operated by CDS in Strasbourg, France, and NASA’s Astrophysics Data System Abstract Service. We used SM plot, by Robert Lupton and Patricia Monger, in the production of some figures. This work made use of data from the European Space Agency (ESA) mission *Gaia* (<https://www.cosmos.esa.int/gaia>), processed by the *Gaia* Data Processing and Analysis Consortium (DPAC). Funding for the DPAC has been provided by national institutions, in particular the institutions participating in the *Gaia* Multilateral Agreement.

⁷ Noted by the anonymous referee.

This research was based in part on observations obtained at the Gemini Observatory, which is operated by the Association of Universities for Research in Astronomy, Inc., under a cooperative agreement with the NSF on behalf of the Gemini partnership: the National Science Foundation (United States), the National Research Council (Canada), CONICYT (Chile), Ministerio de Ciencia, Tecnología e Innovación Productiva (Argentina), and Ministério da Ciência, Tecnologia e Inovação (Brazil). The Phoenix spectrograph was developed by NOAO. IGRINS was developed under a collaboration between the University of Texas at Austin and the Korea Astronomy and Space Science Institute (KASI) with the financial support of the US National Science Foundation under grant AST-1229522, the University of Texas at Austin, and the Korean GMT Project of KASI.

The National Optical Astronomy Observatory is operated by the Association of Universities for Research in Astronomy under cooperative agreement with the National Science Foundation. K.H. and R.J. express their thanks to the Office of Science for support of their research. The research at Tennessee State University was supported in part by the State of Tennessee through its Centers of Excellence program. J.M. has been financed by Polish National Science Centre (NSC) grants 2015/18/A/ST9/00746 and 2017/27/B/ST9/01940 and C.G. by NSC grant SONATA No. DEC-2015/19/D/ST9/02974.

ORCID iDs

Kenneth H. Hinkle  <https://orcid.org/0000-0002-2726-4247>

Francis C. Fekel  <https://orcid.org/0000-0002-9413-3896>

Richard R. Joyce  <https://orcid.org/0000-0003-0201-5241>

Joanna Mikołajewska  <https://orcid.org/0000-0003-3457-0020>

Cezary Gałan  <https://orcid.org/0000-0002-7868-5017>

Thomas Lebzelter  <https://orcid.org/0000-0002-0702-7551>

References

- Asplund, M., Grevesse, N., Sauval, A., & Scott, P. 2009, *ARA&A*, **47**, 481
- Barker, E. S., Evans, D. S., & Laing, J. D. 1967, *RGOB*, **130**, 355
- Bessell, M. S., & Wood, P. R. 1984, *PASP*, **96**, 247
- Bopp, B. W., Evans, D. S., Laing, J. D., & Deeming, T. J. 1970, *MNRAS*, **147**, 355
- Bourgés, L., Lafrasse, S., Mella, G., et al. 2014, in ASP Conf. Ser. 485, *Astronomical Data Analysis Software and Systems XXIII*, ed. N. Manset & P. Forshay (San Francisco, CA: ASP), 223
- Brandt, S. 1998, *Data Analysis, Statistical and Computational Methods for Scientists and Engineers*, Polish edition (Warsaw: Polish Scientific Publishers PWN)
- Brown, J. A., Smith, V. V., Lambert, D. L., et al. 1990, *AJ*, **99**, 1930
- Burrows, D. N., Chester, M. M., Gehrels, N., et al. 2015, *GCN Circ.*, 17280
- Casares, J., Jonker, P. G., & Israelian, G. 2017, in *X-Ray Binaries in Handbook of Supernovae*, ed. A. Alsabti & P. Murdin (New York: Springer), 1499
- Chakrabarty, D., & Roche, P. 1997, *ApJ*, **489**, 254
- Charbonnel, C., Meynet, G., Maeder, A., & Schaerer, D. 1996, *A&AS*, **115**, 339
- Cooke, B. A., Ricketts, M. J., Maccacaro, T., et al. 1978, *MNRAS*, **182**, 489
- Corbet, R. H. D., Sokolowski, J. L., Mukai, K., Markwardt, C. B., & Tueller, J. 2008, *ApJ*, **675**, 1424
- Cutri, R. M., Skrutskie, M. F., van Dyk, S., et al. 2003, *The IRSA 2MASS All-Sky Point Source Catalog*, NASA/IPAC Infrared Science Archive, <http://irsa.ipac.caltech.edu/applications/Gator/>
- dal Fiume, D., Poulsen, J. M., Frontera, F., Manzo, G., & Re, S. 1990, *NCimC*, **13**, 481
- Daniels, W. 1966, *Univ. Maryland Tech. Rep.* 579
- Dewey, R. J., & Cordes, J. M. 1987, *ApJ*, **321**, 780
- Duchêne, G., & Kraus, A. 2013, *ARA&A*, **51**, 269
- Dyck, H. M., Benson, J. A., van Belle, G. T., & Ridgway, S. T. 1996, *AJ*, **111**, 1705
- Eaton, J. A., & Williamson, M. H. 2007, *PASP*, **119**, 886
- Eggleton, P. P. 1983, *ApJ*, **268**, 368
- Enoto, T., Sasano, M., Yamada, S., et al. 2014, *ApJ*, **786**, 127
- Escorza, A., Boffin, H. M. J., Jorissen, A., et al. 2017, *A&A*, **608**, A100
- Famaey, B., Pourbaix, D., Frankowski, A., et al. 2009, *A&A*, **498**, 627
- Fekel, F. C., Joyce, R. R., Hinkle, K. H., & Skrutskie, M. F. 2000, *AJ*, **119**, 1375
- Fekel, F. C., Rajabi, S., Muterspaugh, M. W., & Williamson, M. W. 2013, *AJ*, **145**, 111
- Fekel, F. C., Tomkin, J., & Williamson, M. H. 2009, *AJ*, **137**, 3900
- Fitzpatrick, M. J. 1993, in ASP Conf. Ser. 52, *Astronomical Data Analysis Software and Systems II*, ed. R. J. Hanish, R. J. V. Brissenden, & J. Barnes (San Francisco, CA: ASP), 472
- Forman, W., Jones, C., Cominsky, L., et al. 1978, *ApJS*, **38**, 357
- Freire, P. C. C., & Tauris, T. M. 2014, *MNRAS*, **438**, L86
- Gaia Collaboration, Brown, A. G. A., Vallenari, A., et al. 2018, *A&A*, **616**, A1
- Gałan, C., Mikołajewska, J., Hinkle, K. H., & Joyce, R. R. 2016, *MNRAS*, **455**, 1282
- Gałan, C., Mikołajewska, J., Hinkle, K. H., & Joyce, R. R. 2017, *MNRAS*, **466**, 2194
- Galloway, D. K., Sokolowski, J. L., & Kenyon, S. J. 2002, *ApJ*, **580**, 1065
- Garcia, M., Baliunas, S. L., Doxsey, R., et al. 1983, *ApJ*, **267**, 291
- Gaudenzi, S., & Polcaro, V. F. 1999, *A&A*, **347**, 473
- González-Galán, A., Kuulkers, E., Kretschmar, P., et al. 2012, *A&A*, **537**, A66
- Goorvitch, D. 1994, *ApJS*, **95**, 535
- Goranskij, V. P., Metlova, N. V., & Barsukova, E. A. 2012, *AstBu*, **67**, 73
- Gromadzki, M., Mikołajewska, J., & Soszyński, I. 2013, *AcA*, **63**, 405
- Gustafsson, B., Edvardsson, B., Eriksson, K., et al. 2008, *A&A*, **486**, 951
- Hall, D. N. B., Ridgway, S. T., Bell, E. A., & Yarbrough, J. M. 1978, *Proc. SPIE*, **172**, 121
- Hartig, E., Cash, J., Hinkle, K. H., et al. 2014, *AJ*, **148**, 123
- Hinkle, K. H., Cuberly, R. W., Gaughan, N. A., et al. 1998, *Proc. SPIE*, **3354**, 810
- Hinkle, K. H., Fekel, F. C., Joyce, R. R., et al. 2006, *ApJ*, **641**, 479
- Hinkle, K. H., Fekel, F. C., & Joyce, R. R. 2009, *ApJ*, **692**, 1360
- Hinkle, K. H., Hall, D. N. B., & Ridgway, S. T. 1982, *ApJ*, **252**, 697
- Hinkle, K. H., Lebzelter, T., Joyce, R. R., & Fekel, F. C. 2002, *AJ*, **123**, 1002
- Hinkle, K. H., Lebzelter, T., & Straniero, O. 2016, *ApJ*, **825**, 38 (HLS16)
- Iben, I., & Tutukov, A. V. 1999, *ApJ*, **511**, 324
- Ilkiewicz, K., Mikołajewska, J., & Monard, B. 2017, *A&A*, **601**, A105
- Jorissen, A., Frankowski, A., Famaey, B., & Van Eck, S. 2009, *A&A*, **498**, 489
- Joyce, R. R. 1992, in ASP Conf. Ser. 23, *Astronomical CCD Observing and Reduction Techniques*, ed. S. B. Howell (San Francisco, CA: ASP), 258
- Joyce, R. R., Hinkle, K. H., Meyer, M. R., & Skrutskie, M. F. 1998, *Proc. SPIE*, **3354**, 741
- Kazarovets, E. V., Samus, N. N., Durlevich, O. V., et al. 1999, *IBVS*, **4659**, 1
- Krimm, H. A., Kennea, J. A., Burrows, D. N., et al. 2014, *ATel*, **6482**
- Kupka, F., Piskunov, N., Ryabchikova, T. A., Stempels, H. C., & Weiss, W. W. 1999, *A&AS*, **138**, 119
- Lambert, D. L. 1987, *JApA*, **8**, 103
- Lebzelter, T., Mowlavi, N., Marigo, P., et al. 2018, *A&A*, **616**, L13
- Liu, Q. Z., van Paradijs, J., & van den Heuvel, E. P. J. 2007, *A&A*, **469**, 807
- Lorimer, D. R., & McLaughlin, M. A. 2006, *HiA*, **14**, 119
- Lü, G.-L., Zhu, C.-H., Postnov, K. A., et al. 2012, *MNRAS*, **424**, 2265
- Lyne, A. G., & Lorimer, D. R. 1994, *Natur*, **369**, 127
- Majewski, S. R. & APOGEE Team & APOGEE-2 Team 2016, *AN*, **337**, 863
- Masetti, N., Dal Fiume, D., Cusumano, G., et al. 2002, *A&A*, **382**, 104
- Masetti, N., Orlandini, M., Palazzi, E., Amati, L., & Frontera, F. 2006, *A&A*, **453**, 295
- Mélandez, J., & Barbuy, B. 1999, *ApJS*, **124**, 527
- Mürset, U., Wolff, B., & Jordan, S. 1997, *A&A*, **319**, 201
- Nicholls, C. P., Wood, P. R., Dioni, M.-R. L., & Soszyński, I. 2009, *MNRAS*, **399**, 2063
- Nucita, A. A., Stefanelli, S., De Paolis, F., et al. 2014, *A&A*, **562**, A55
- Ohnaka, K., Scholz, M., & Wood, P. R. 2006, *A&A*, **446**, 1119
- Park, C., Jaffe, D. T., Yuk, I.-S., et al. 2014, *Proc. SPIE*, **9147**, 91471D
- Ridgway, S. T., & Hinkle, K. H. 1987, in *The Impact of Very High S/N Spectroscopy on Stellar Physics*, ed. M. Spite (Dordrecht: Reidel), 61
- Saio, H., Wood, P. R., Takayama, M., & Ita, Y. 2015, *MNRAS*, **452**, 3863
- Scarfe, C. D., Batten, A. H., & Fletcher, J. M. 1990, *PDAO*, **18**, 21
- Schlafly, E. F., & Finkbeiner, D. P. 2011, *ApJ*, **737**, 103
- Schmidt, M. R., Začs, L., Mikołajewska, J., & Hinkle, K. H. 2006, *A&A*, **446**, 603
- Scott, P., Asplund, M., Grevesse, N., et al. 2015a, *A&A*, **573**, 26
- Scott, P., Grevesse, N., Asplund, M., et al. 2015b, *A&A*, **573**, 25

- Shetrone, M., Bizyaev, D., Lawler, J. E., et al. 2015, *ApJS*, **221**, 24
- Si, S., van Dyk, D. A., von Hippel, T., et al. 2018, *MNRAS*, **480**, 1300
- Smith, V. 1990, *MmSAI*, **61**, 787
- Snedden, C., Lucatello, S., Ram, R. S., Brooke, J. S. A., & Bernath, P. 2014, *ApJS*, **214**, 26
- Sokoloski, J. L., Bildsten, L., & Ho, W. C. G. 2001, *MNRAS*, **326**, 553
- Soszyński, I. 2007, *ApJ*, **660**, 1486
- Soszyński, I., Dziembowski, W. A., Udalski, A., et al. 2007, *AcA*, **57**, 201
- Stothers, R. B. 2010, *ApJ*, **725**, 1170
- Taam, R. E., & Sandquist, E. L. 2000, *ARA&A*, **38**, 113
- Takayama, M., Wood, P. R., & Ita, Y. 2015, *MNRAS*, **448**, 464
- Tauris, T. M., & van den Heuvel, E. P. J. 2006, in *Compact stellar X-ray Sources*, ed. W. Lewin & M. van der Klis (Cambridge: Cambridge Univ. Press), 623
- Thorsett, S. E., & Chakrabarty, D. 1999, *ApJ*, **512**, 288
- Tiengo, A., Galloway, D. K., di Salvo, T., et al. 2005, *A&A*, **441**, 283
- Tomasella, L., Munari, U., Tomov, T., et al. 1997, *IBVS*, 4537
- Trabucchi, M., Wood, P. R., Montalb'an, J., et al. 2017, *ApJ*, **847**, 139
- Tsuji, T. 1988, *A&A*, **197**, 185
- van Belle, G. T., Lane, B. F., Thompson, R. R., et al. 1999, *AJ*, **117**, 521
- Vassiliadis, E., & Wood, P. 1993, *ApJ*, **413**, 641
- Wallace, L., & Hinkle, K. H. 1997, *ApJS*, **111**, 445
- Wijnands, R., & van der Klis, M. 1998, *Natur*, **394**, 344
- Wiktorowicz, G., Sobolewska, M., Lasota, J.-P., & Belczynski, K. 2017, *ApJ*, **846**, 17
- Willems, B., & Kolb, U. 2002, *MNRAS*, **337**, 1004
- Wood, P. R. 2000, *PASA*, **17**, 18
- Wood, P. R., Alcock, C., Allsman, R. A., et al. 1999, in *IAU Symp. 191, Asymptotic Giant Branch Stars*, ed. T. Le Bertre, A. Lebre, & C. Waelkens (San Francisco, CA: ASP), 151
- Wood, P. R., & Nicholls, C. P. 2009, *ApJ*, **707**, 573
- Zhu, C., Lü, G., Wang, Z., & Wang, N. 2012, *PASP*, **124**, 195